SUPPORTING INFORMATION

Ligand decorated nickel-based nanoparticles supported onto MXene in catalytic hydrogenation of N-heterocycles

Judith Medina-Vargas,[a] Santiago Martín,[b,c,d] Iván Sorribes,[a] Hermenegildo García[e] and Jose A. Mata[a]**

[a]Institute of Advanced Materials (INAM), Universitat Jaume I, Avda. Sos Baynat s/n, 12071, Castellón, Spain. Tel: +34 964387516. Email: jmata@uji.es

[b]Instituto de Nanociencia y Materiales de Aragón (INMA), CSIC-Universidad de Zaragoza, 50009, Zaragoza, Spain.

[c]Departamento de Química Física, Universidad de Zaragoza, 50009, Zaragoza, Spain.

[d]Laboratorio de Microscopias Avanzadas (LMA). Universidad de Zaragoza, Edificio I+D+i. 50018, Zaragoza, Spain.

[e]Instituto de Tecnología Química, Consejo Superior de Investigaciones Científicas-Universitat Politècnica de València. Avda. Los Naranjos s/n, 46022, Valencia (Spain)

Contents

S1. Catalysts comparison in hydrogenation of N-heterocycles

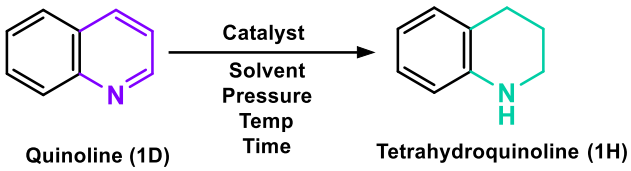

Table S1 Comparison of **NiNPs/NHC@MXene** with benchmark nickel-based systems

	Catalyst	Ni loading	Solvent	H_2 source	T (°C)	t (h)	Yield	Rec.	Reg.	Ref.
1	$NiCl_2{\cdot}6H_2O$/Ligand	1 mol%	MeOH	$NH_3{\cdot}BH_3$	25	24	90	-	No	[7]
2	Ni@hw-mSiO_2	0.12 g/12%	EtOH	H_2 (30 bar)	100	2	96	6	No	[8]
3	Ni-NPs@NBC-700	16 mol%	*i*PrOH	H_2 (30 bar)	120	24	99	5	No	[9]
4	Ni-CeO_x/CN-550	1.6 mol%	MeOH	H_2 (20 bar)	120	24	99	5	No	[10]
5	Ni-phen@SiO_2-1000	4.5 mol%	H_2O/MeOH	H_2 (50 bar)	120	20	87	5	No	[11]
6	Ni-phen@SiO_2-800	4 mol%	H_2O/MeOH	H_2 (30 bar)	140	24	92	5	No	[12]
7	Ni/meso-SiO_2-550	8.1 mol%	H_2O/iPrOH	H_2 (10 bar)	60	24	96	5	No	[13]
8	Ni@PC-900-1-4%	4 mol%	H_2O/MeOH	$NH_3{\cdot}BH_3$	25	3.5	99	8	No	[14]
9	**NiNPs/NHC@MXene**	3.7 mol%	EtOH	H_2 (30 bar)	120	17	99	5	Yes	This work

Rec. = recycling; Reg. = regeneration

S2. Example of a gas chromatography analysis in the hydrogenation of quinoline to tetrahydroquinoline.

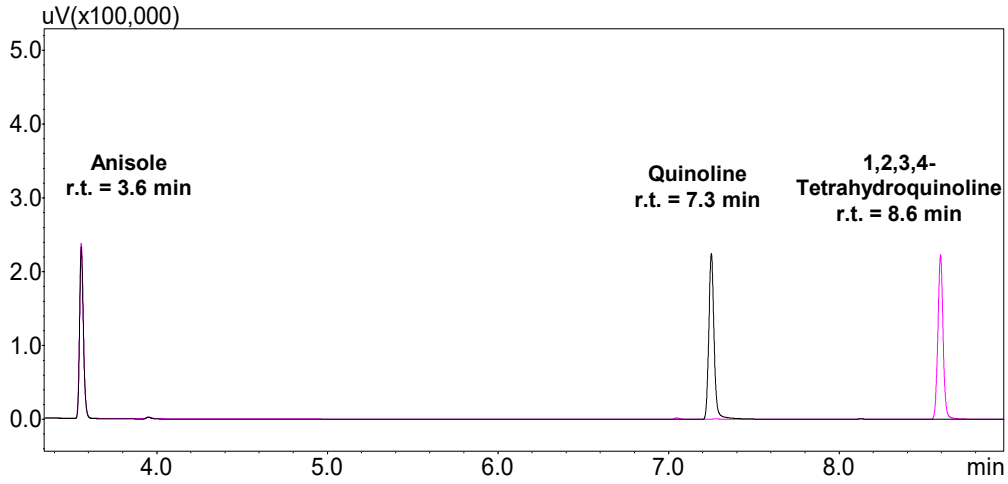

Figure S1 Representative reaction progress by GC/FID in the hydrogenation of quinoline (**1D**, r.t. = 7.3 min) to 1,2,3,4-tetrahydroquinoline (**1H**, r.t. = 8.6 min) in the presence of 0.1 mmol of anisole as an internal standard (r.t. = 3.6 min). Black line: 0h; pink line: 17h.

S3. Example of a calibration curve by GC-FID

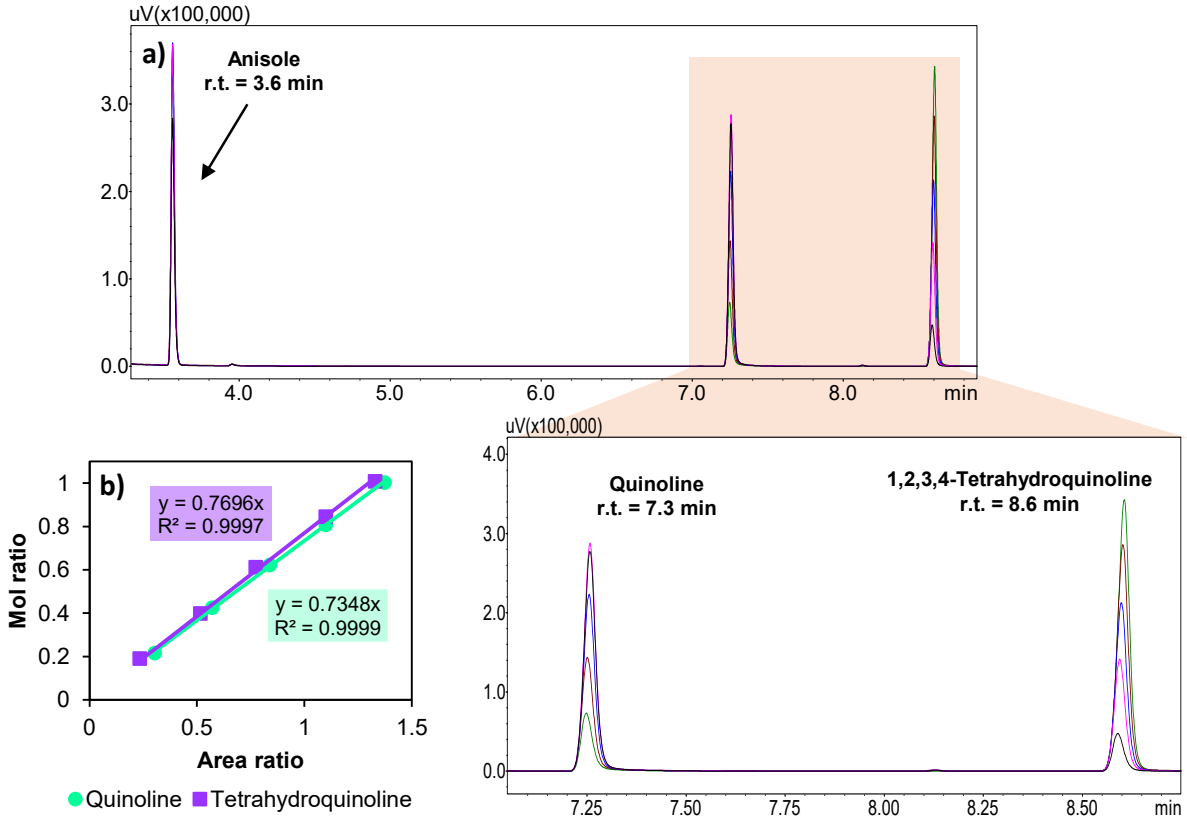

Figure S2 a) GC-FID chromatograms for quinoline (**1D**) and 1,2,3,4-tetrahydroquinoline (**1H**) in different concentrations, using anisole as the internal standard and **b)** Calibration curves.

To quantify the obtained products, we determine calibration curves using anisole as an internal standard (**Figure S2.b**). Solutions with known concentrations of the quinoline, tetrahydroquinoline and internal standard were prepared, and measurements were performed by GC-FID (**Figure S2.a**). The moles of product were calculated using the slope of the curve, the moles of standard (n_{st}), the area ratio between the product (A_P) and the standard (A_{st}) using the following equation:

$$n_P = \text{slope} \times \left(\frac{A_P}{A_{st}} \times n_{st}\right)$$

n_P = moles of product
A_P = Area of product
A_{st} = Area of standard
n_{st} = moles of standard

Once the moles of products and reactants are obtained, the percentages of conversion and yields were calculated with the following equations:

$$\%\text{Conv} = \frac{n_{R,\text{initial}} - n_{R,\text{final}}}{n_{R,\text{initial}}} \times 100 \ , \qquad \%\text{Yield} = \frac{n_P}{n_{R,\text{initial}}} \times 100$$

n_R = moles of reactant
n_P = moles of product

S4. Synthesis and characterization of complex 1

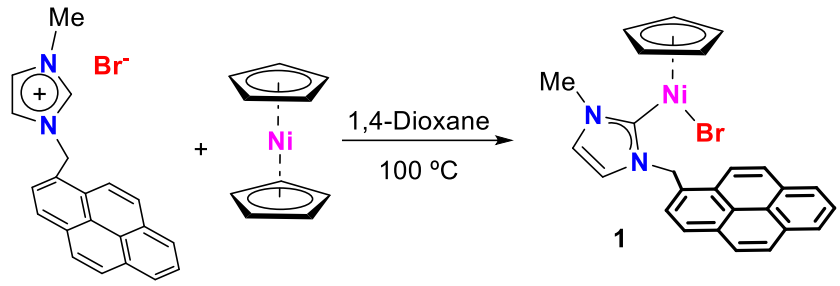

Scheme S1 Synthesis of complex **1**.

Complex **1** was synthesized following a previously reported procedure by our group.[1] The general procedure involved heating a mixture of the bromide of methyl-methylpyrene-imidazolium salt[2] (300 mg, 0.79 mmol) and bis(cyclopentadienyl)nickel(II) (150 mg, 0.79 mmol) at 100 ˚C for 17 hours in dry 1,4-dioxane. Upon completion, the reaction mixture was cooled to room temperature and the remaining solids were removed by filtration. The filtrate was concentrated under reduced pressure, and the product was precipitated by the addition of pentane (5 mL). The resulting red crystalline solid was collected by filtration, washed with pentane (3 x 2 mL) and dried under vacuum. Yield: 205 mg (52%).

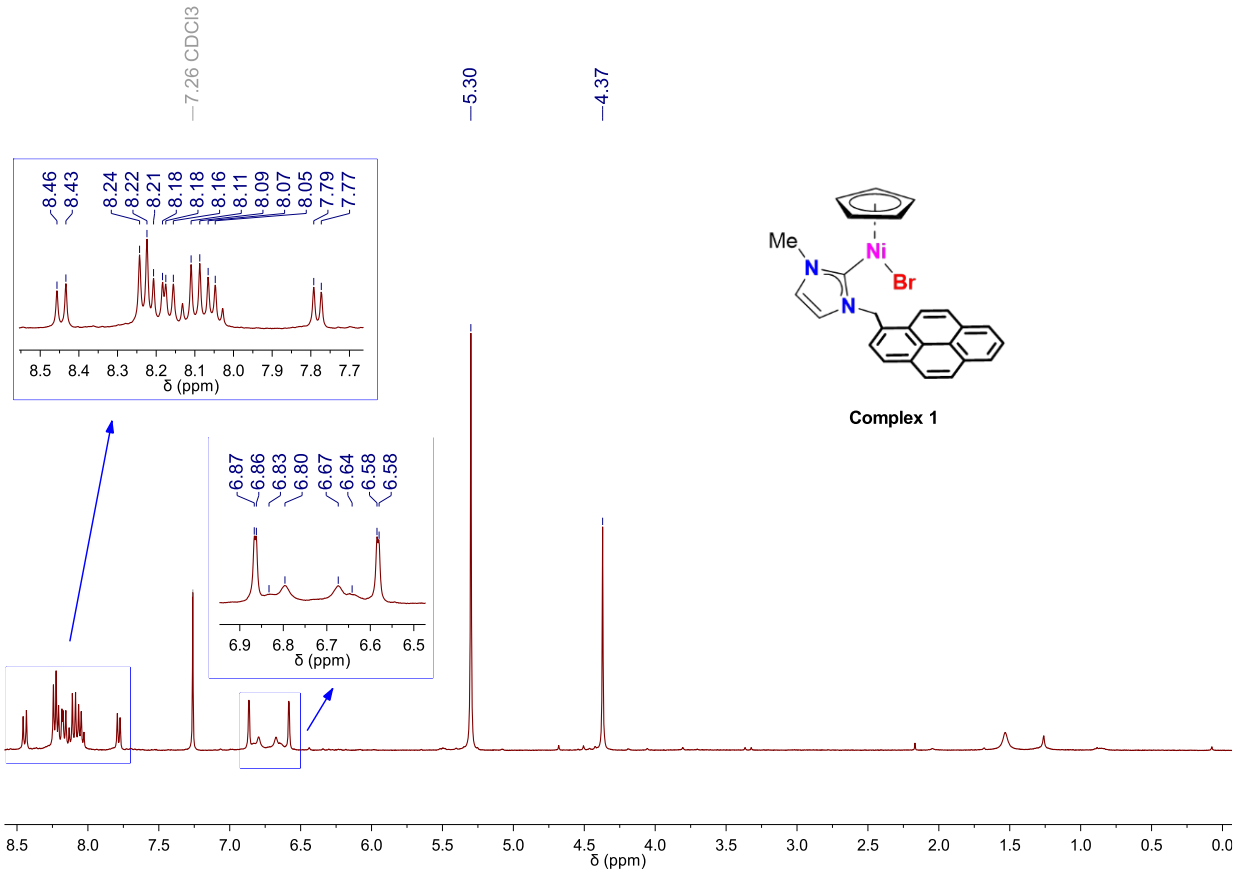

Figure S3 ^{1}H-NMR spectrum of complex **1** in $CDCl_3$. ^{1}H NMR (400 MHz, $CDCl_3$) δ 8.45 (d, $^{3}J_{H,H}$ = 9.3 Hz, 1H, CH_{pyr}), 8.24 – 8.05 (m, 7H, CH_{pyr}), 7.79 (d, $^{3}J_{H,H}$ = 7.9 Hz, 1H, CH_{pyr}), 6.87 (d, $^{3}J_{H,H}$ = 1.7 Hz, 1H, C$H_{imidazole}$), 6.83 (d, $^{3}J_{H,H}$ = 13.4 Hz, 1H, NCH_aH$_b$–), 6.63 (d, $^{3}J_{H,H}$ = 13.4 Hz, 1H, NCH$_a$$H_b$–), 6.58 (d, $^{3}J_{H,H}$ = 1.7 Hz, 1H, CH$_{imidazole}$), 5.30 (s, 5H, CH_{cp}), 4.37 (s, 3H, NCH_3).

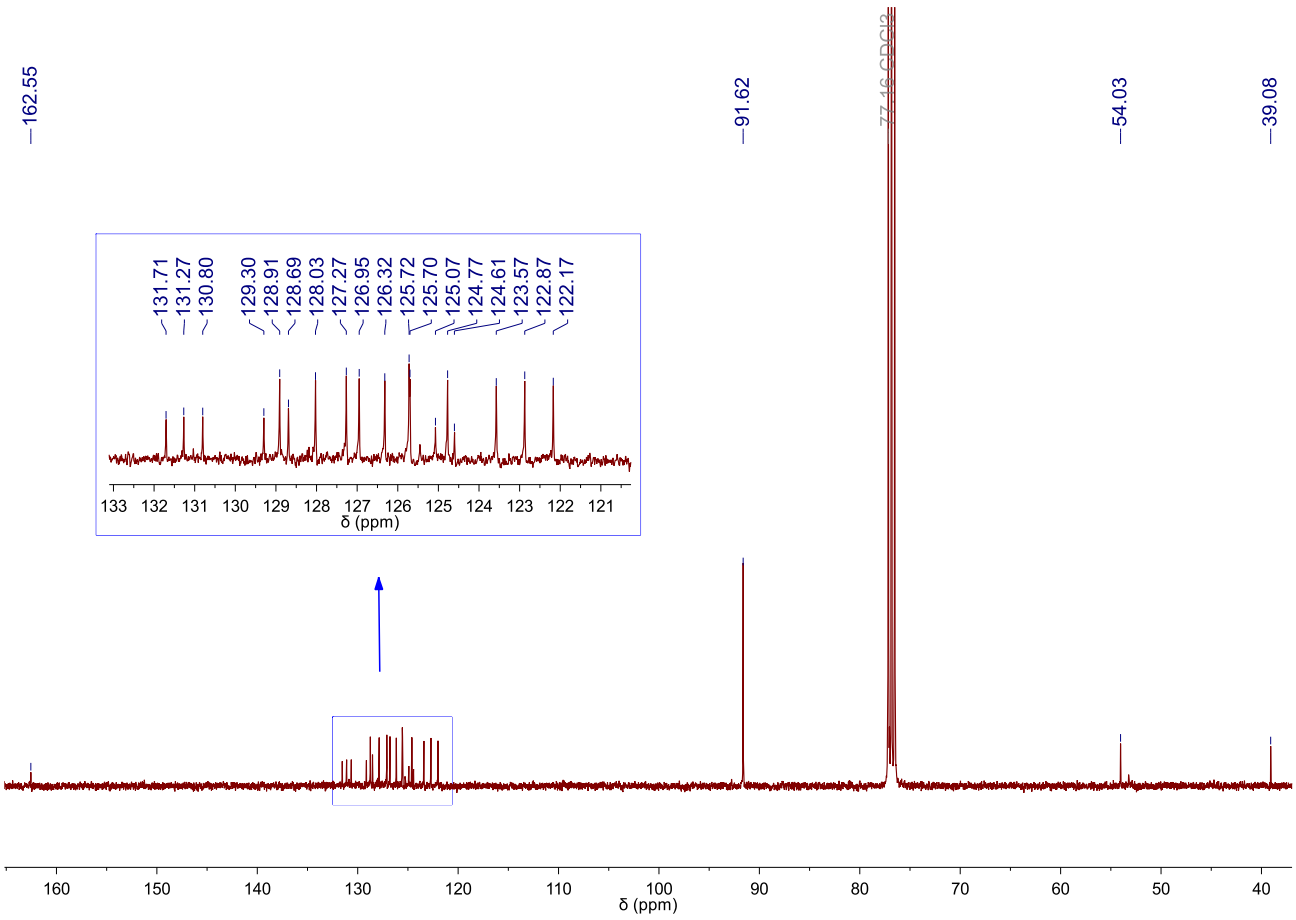

Figure S4 $^{13}C\{^{1}H\}$-NMR spectrum of complex **1** in $CDCl_3$. $^{13}C\{^{1}H\}$ NMR (100 MHz, $CDCl_3$) δ 162.3 ($C_{carbene}$–Ni), [131.7, 131.3, 130.8, 129.3, 128.9, 128.7, 128.0, 127.3, 127.0, 126.3, 125.7, 125.5, 125.1, 124.8, 124.6, 123.6, 122.9, 122.2] (CH_{pyr}, $CH_{imidazole}$), 91.6 (CH_{cp}), 54.0 (NCH_2–), 39.1 (NCH_3).

S5. Scanning electron microscopy (SEM) of Ti_3AlC_2 MAX phase and Ti_3C_2 MXene

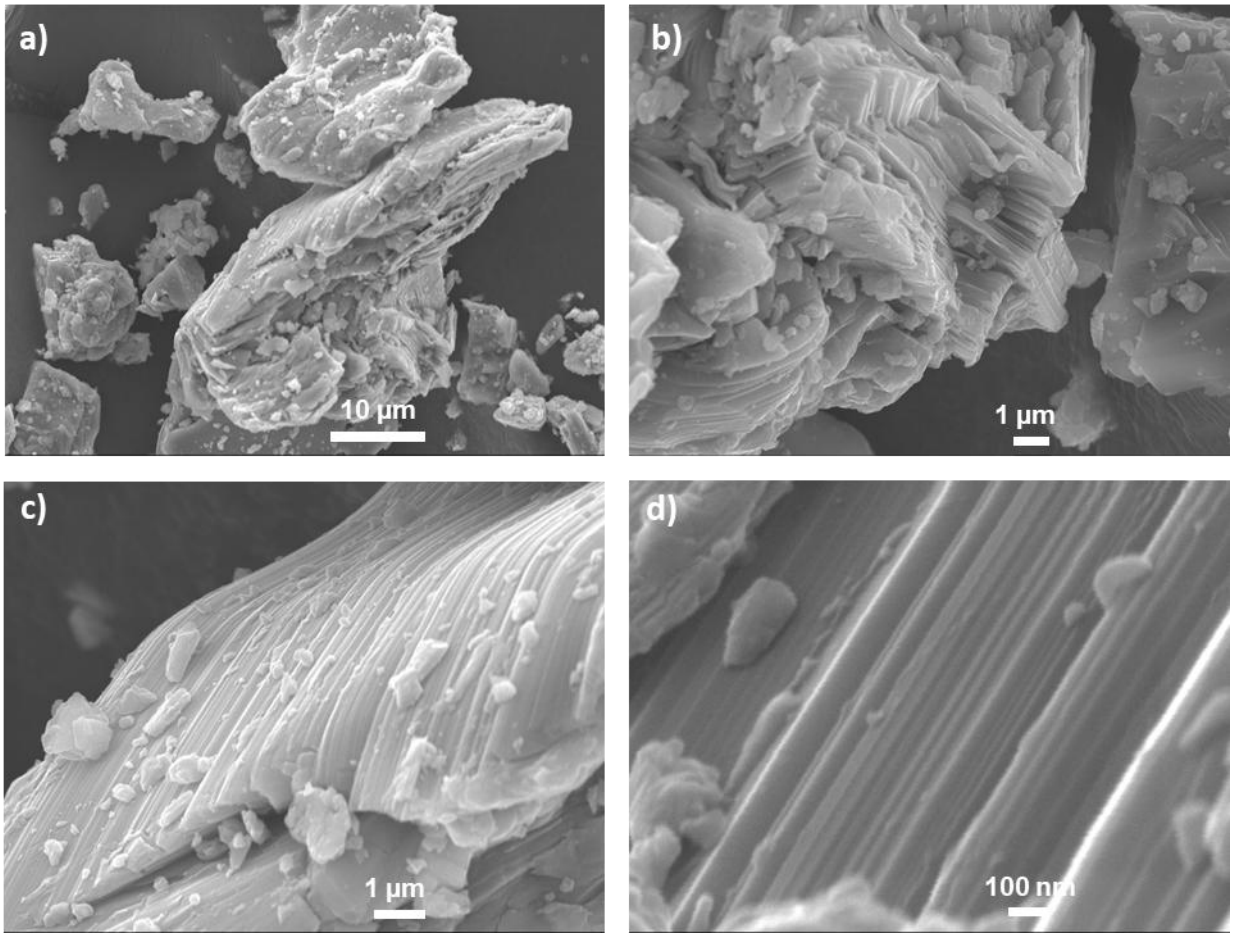

Figure S5 SEM images of the **Ti_3AlC_2 MAX phase** at different magnifications

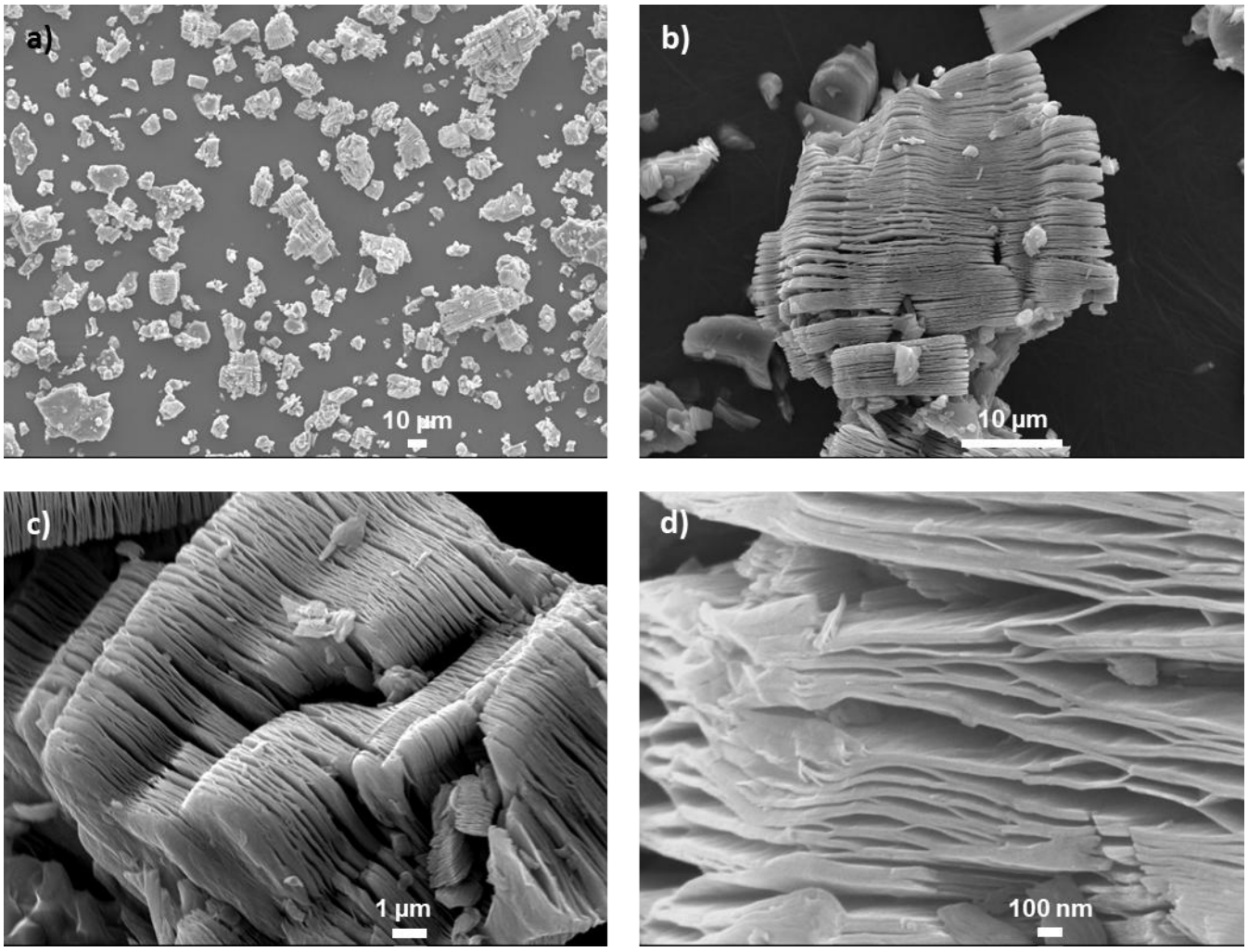

Figure S6 SEM images of the **Ti_3C_2 MXene** at different magnifications.

S6. High resolution transmission electron microscopy (HRTEM)

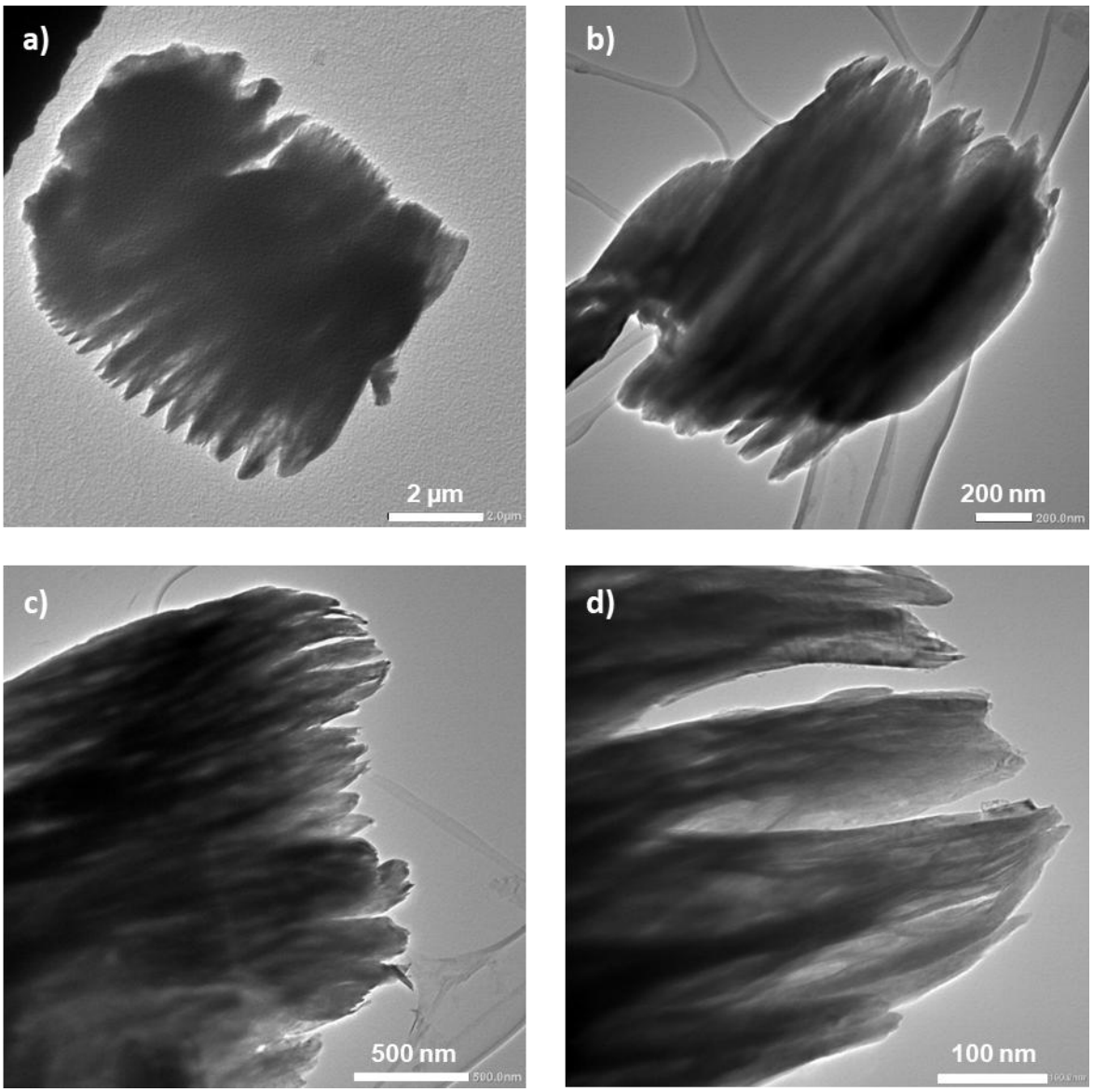

Figure S7 HRTEM images of the **Ti_3C_2 MXene** at different magnifications

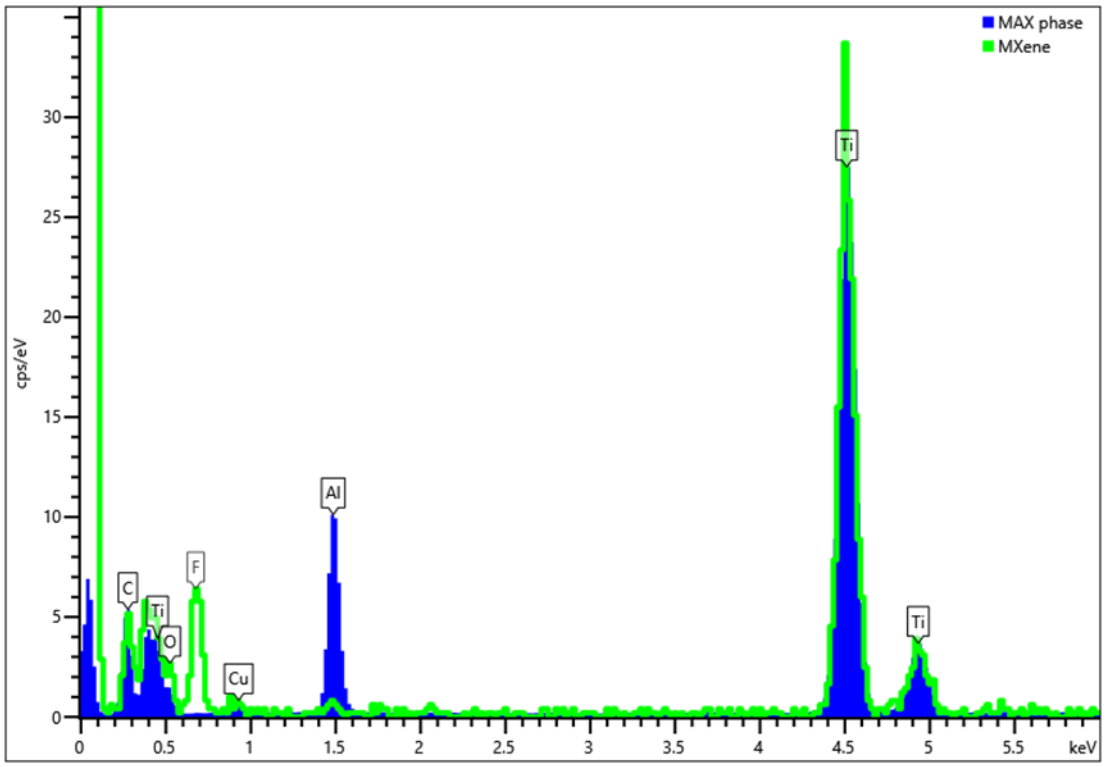

Figure S8 EDX comparison analysis of the **Ti_3AlC_2 MAX phase** (blue) and the **Ti_3C_2 MXene** (green) showing the decrease of aluminum and the emergence of fluorine following the HF etching process.

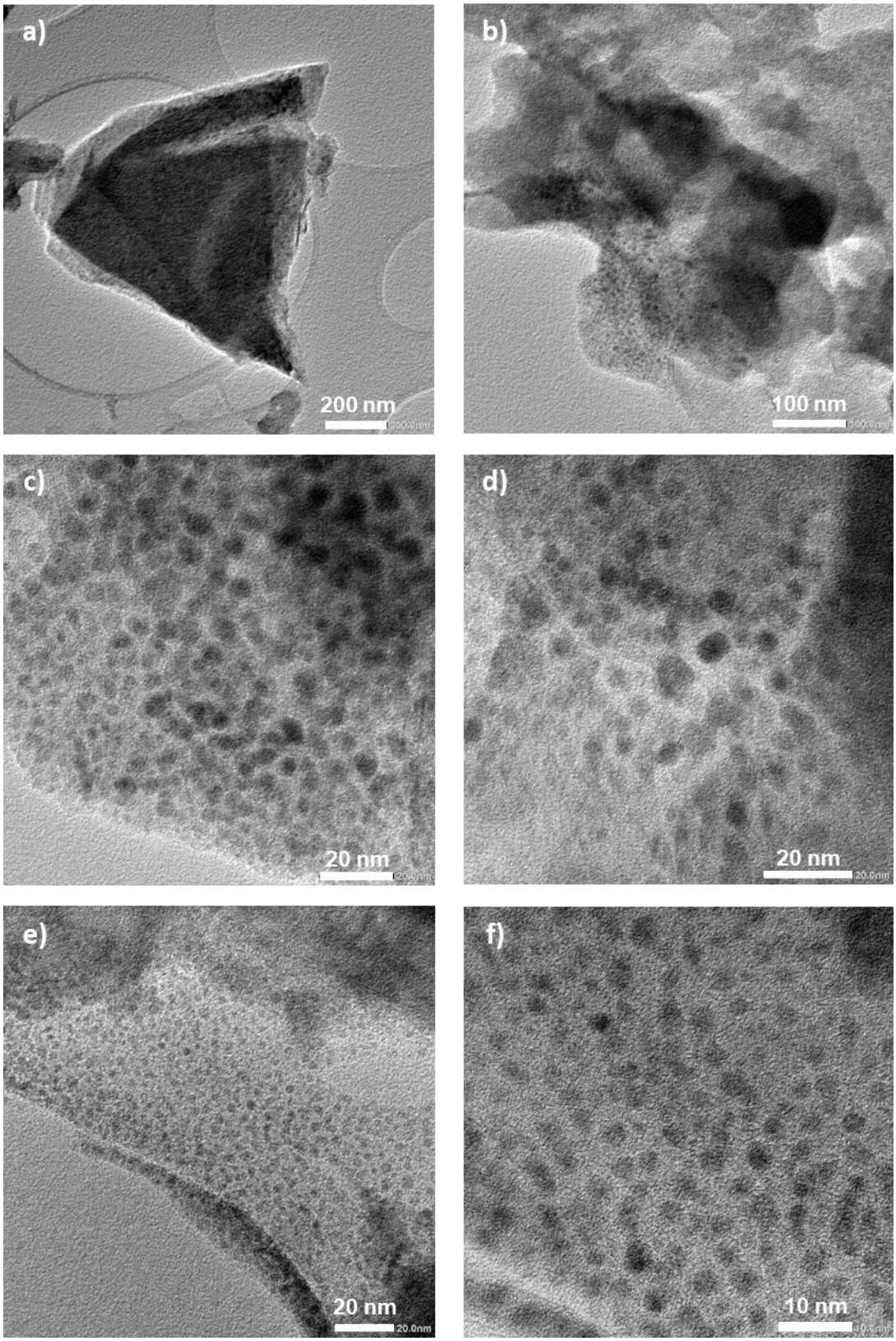

Figure S9 HRTEM images of **NiNPs/NHC@MXene** at different magnifications

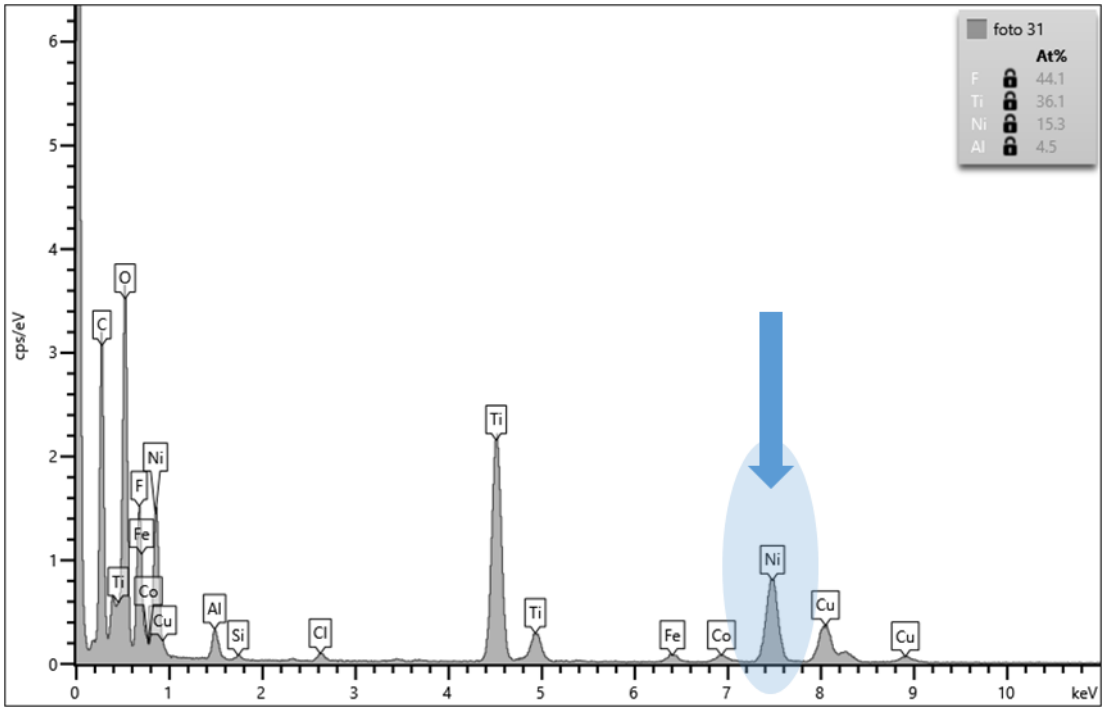

Figure S10 EDX analysis of **NiNPs/NHC@MXene** showing the presence of nickel. The presence of copper is from the grid used in HRTEM analysis.

S7. X-ray photoelectron spectroscopy (XPS)

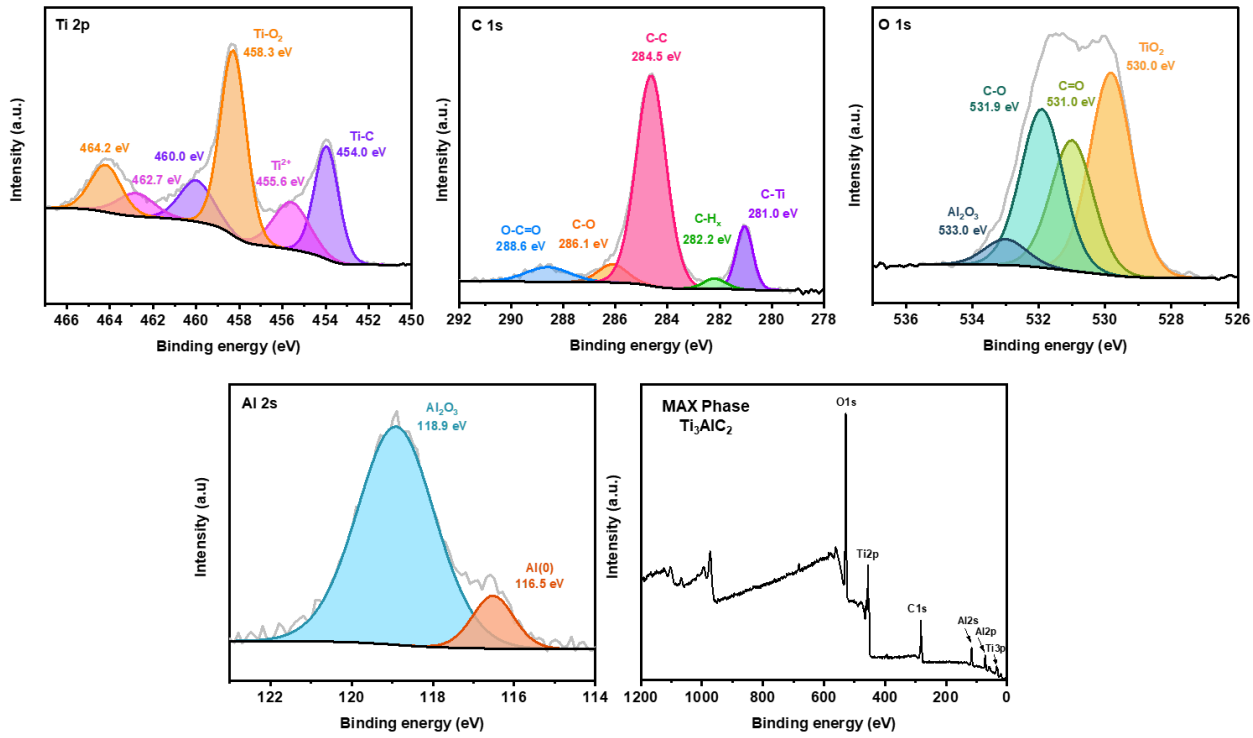

Figure S11 XPS analysis of the **Ti_3AlC_2 MAX phase** showing the high-resolution core-level peaks of Ti, C, O and Al and the survey spectrum.

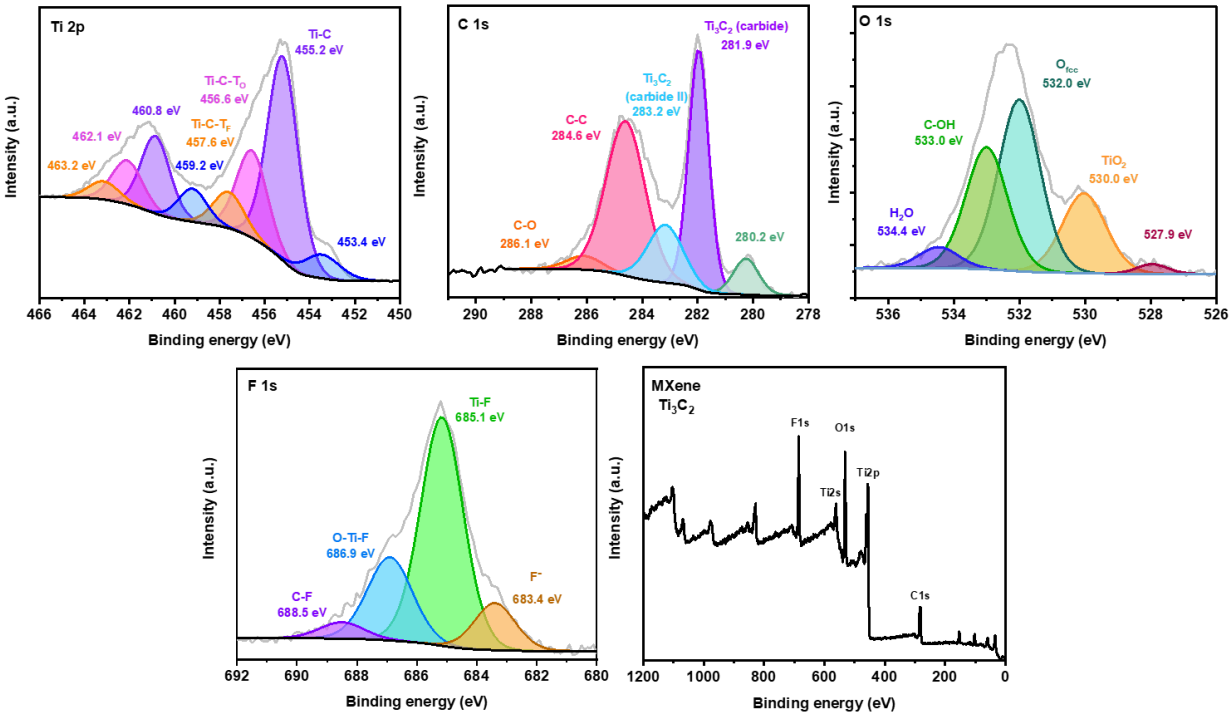

Figure S12 XPS analysis of the **Ti_3C_2 MXene** showing the high-resolution core-level peaks of Ti, C, O and F and the survey spectrum.

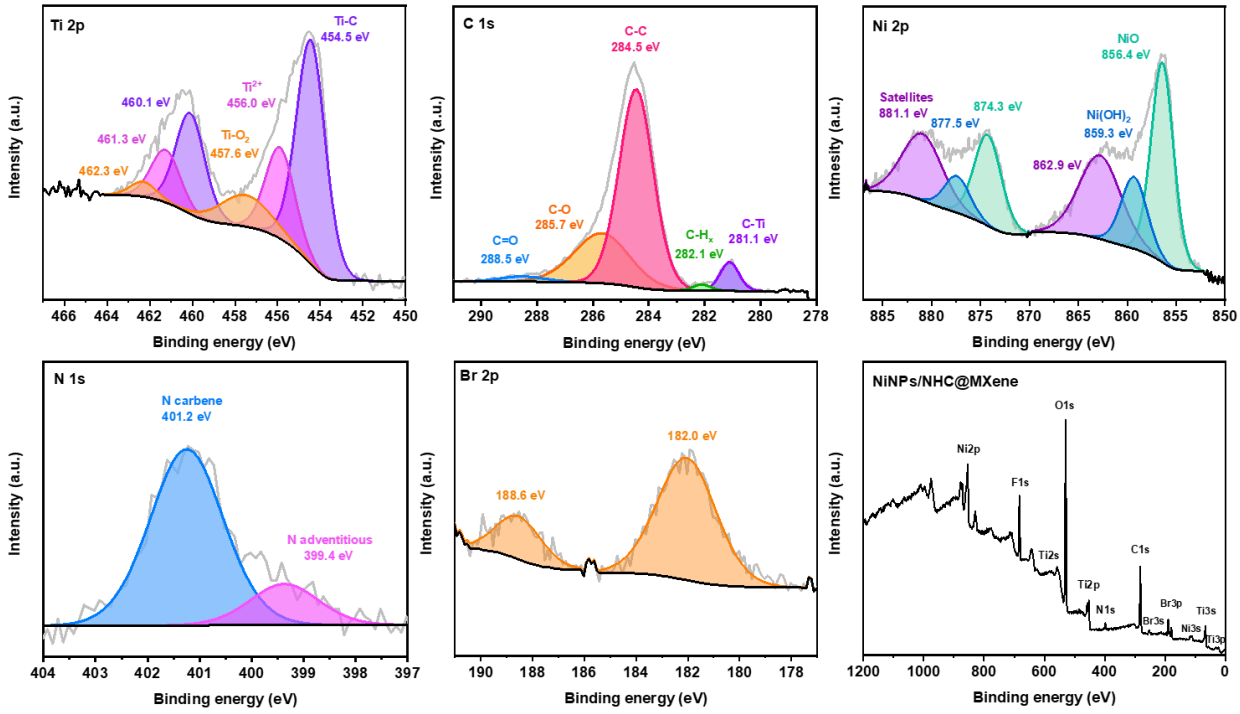

Figure S13 XPS analysis of the **NiNPs/NHC@MXene**.

S8. Characterization of NiNPs/MXene

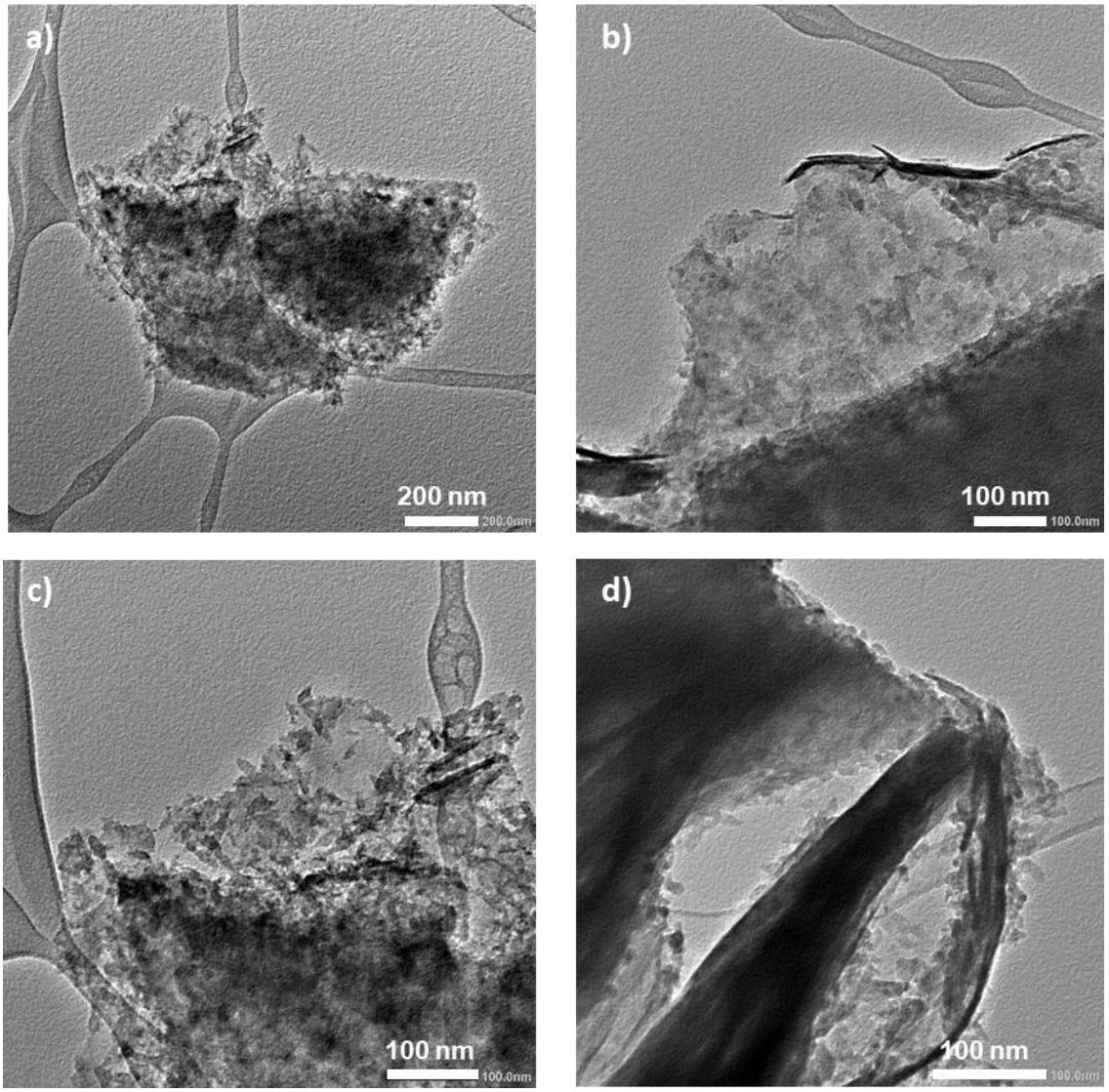

Figure S14 HRTEM images of **NiNPs@MXene** at different magnifications

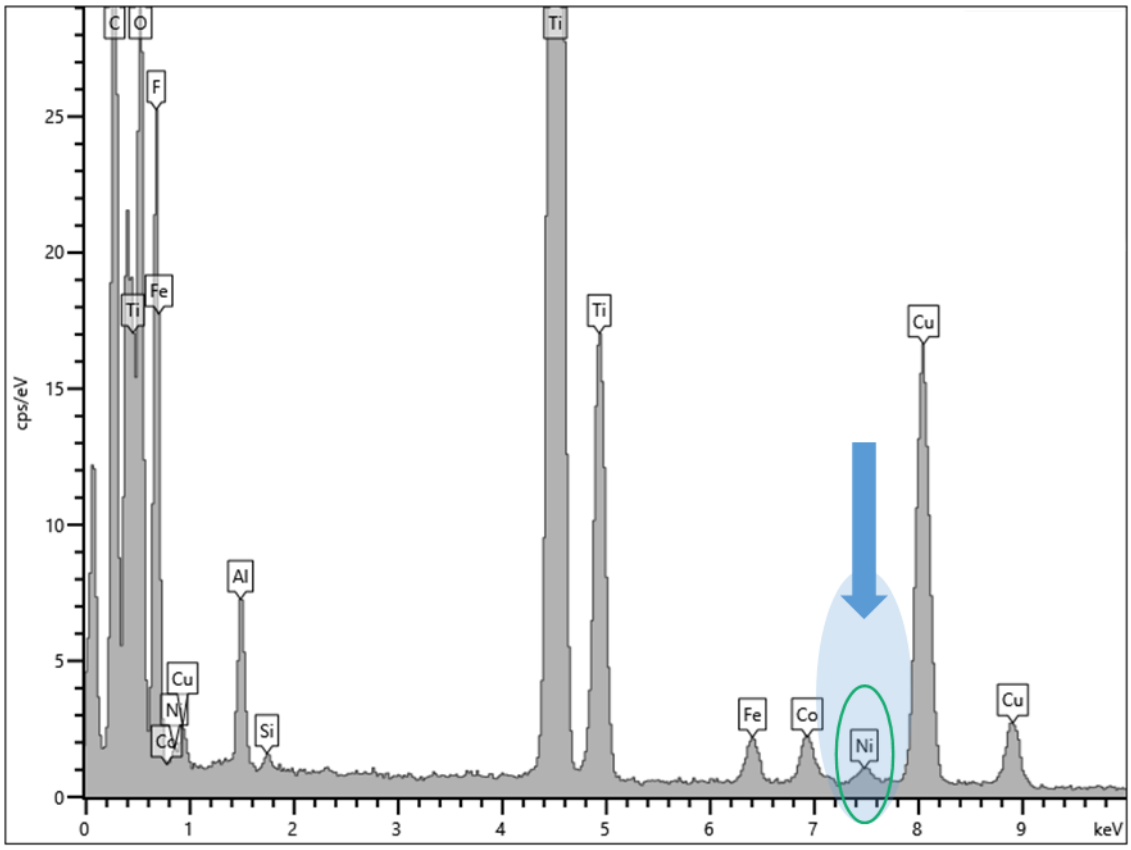

Figure S15 EDX analysis of **NiNPs@MXene** showing the presence of nickel. The presence of copper is from the grid used in HRTEM analysis.

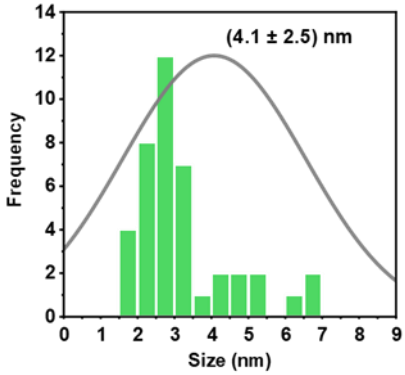

Figure S16 Size histogram of **NiNPs@MXene** (N = 100).

S9. Synthesis and characterization of complex 2 and NiNPs/Me_2NHC@MXene.

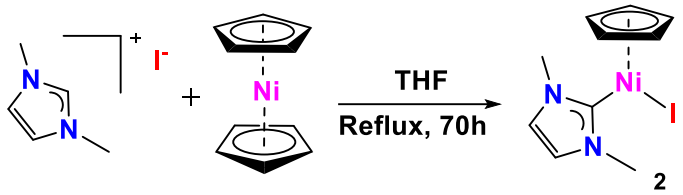

Scheme S2 Synthesis of complex **2**.

The synthesis was adapted by a previously reported procedure.[3] A mixture of the 1,3-dimethylimidazolium iodide (177 mg, 0.79 mmol) and bis(cyclopentadienyl)nickel(II) (150 mg, 0.79 mmol) was refluxed for 63h in THF during which time the solution color slowly changed from a dark green to a dark red. The reaction mixture was filtered through celite using a cannula transfer process, and the filtrate was concentrated under reduced pressure. The resulting red solid was redissolved in the minimum amount of CH_2Cl_2, precipitated with pentane, and isolated by filtration. Formula: $C_{10}H_{13}N_2INi$. Yield: 156.2 mg (57%).

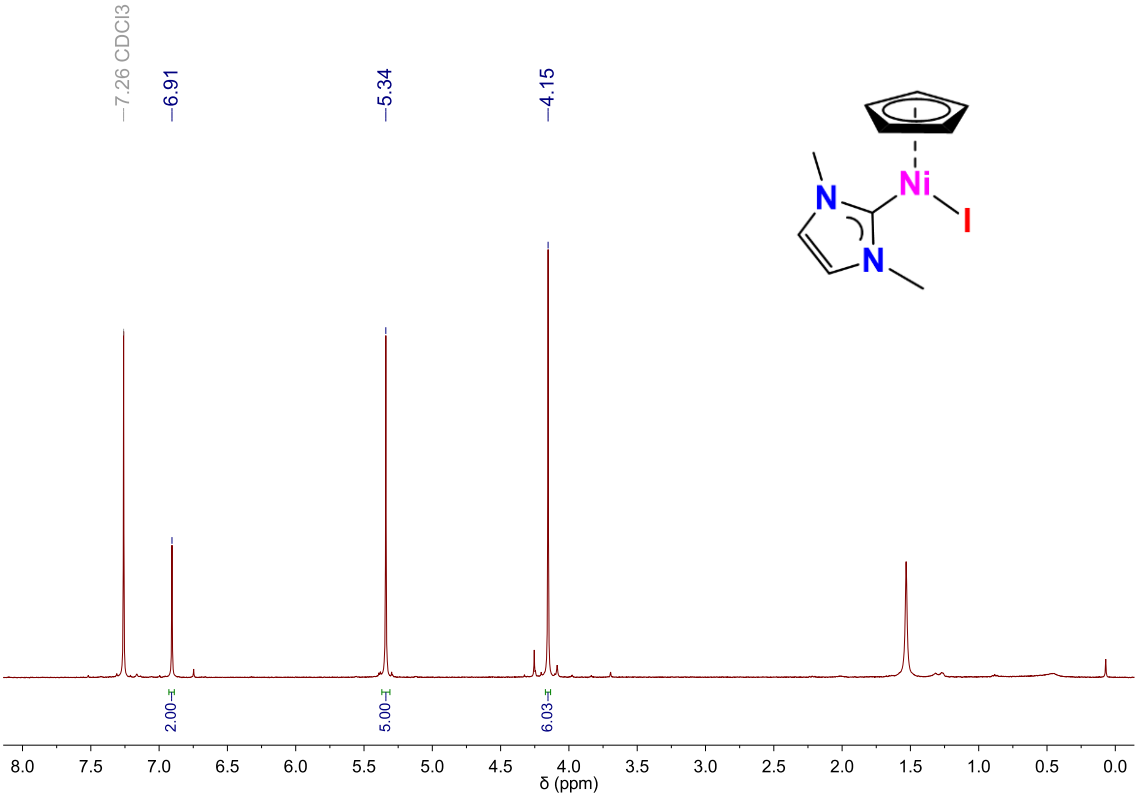

Figure S17 ^{1}H-NMR spectrum of complex **2** in $CDCl_3$. ^{1}H NMR (400 MHz, $CDCl_3$) δ 6.91(s, 2H, CH_{imid}), δ 5.34(s, 5H, CH_{Cp}), δ 4.15 (s, 6H, NCH_3).

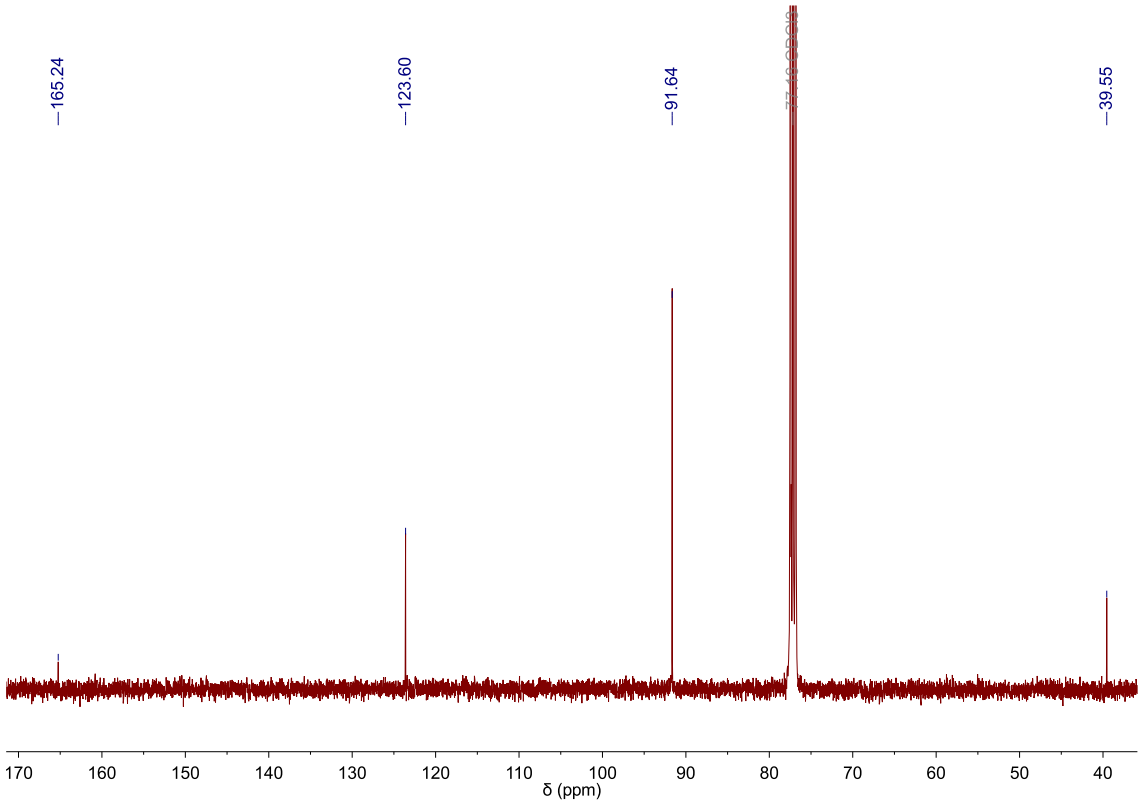

Figure S18 $^{13}C\{^{1}H\}$-NMR spectrum of complex **2** in $CDCl_3$. $^{13}C\{^{1}H\}$ NMR (100 MHz, $CDCl_3$) δ 165.24 ($C_{carbene}$–Ni), δ 123.6 (CH_{imid}), δ 91.64 (CH_{cp}), δ 39.55 (NCH_3).

Synthesis of NiNPs/Me₂NHC@MXene. Ti_3C_2 powder (82 mg) was dispersed in a round-bottom flask with CH_2Cl_2 (10 mL) and sonicated for 30 minutes to ensure homogeneous suspension. Separately, complex **2** (18 mg) was dissolved in CH_2Cl_2 (2 mL) and was then added to the Ti_3C_2 suspension. The resulting mixture was sonicated for an additional 5 minutes time. To induce the formation of nanoparticles, 1 equiv. of tert-butylamine borane ($^{t}BuNH_2{\cdot}BH_3$), dissolved in 3 mL CH_2Cl_2, was added dropwise to the mixture under continuous stirring. The reaction mixture was then stirred at room temperature for 20 hours under a nitrogen atmosphere. After this time, the material was recovered by filtration, washed thoroughly with CH_2Cl_2 (3 x 5 mL), and dried under reduced pressure.

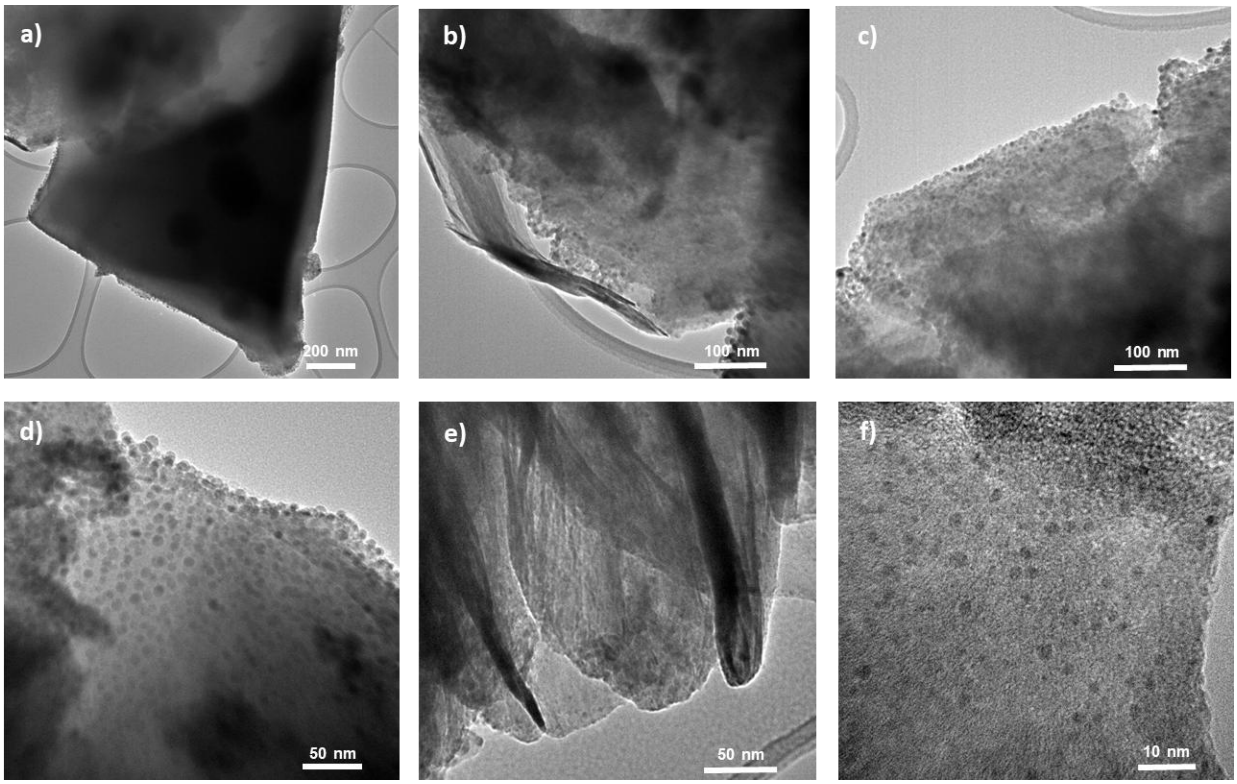

Figure S19 HRTEM images of **NiNPs/Me$_2$NHC@MXene** at different magnifications

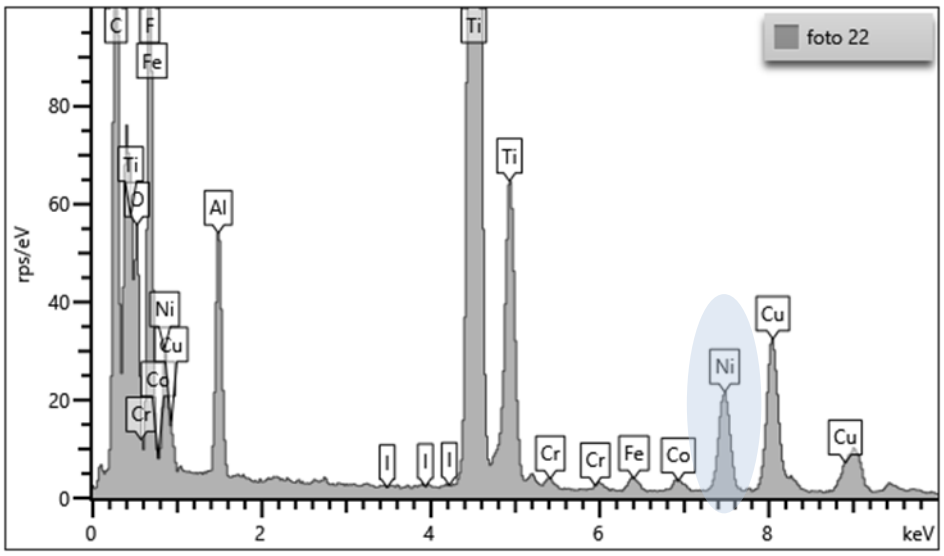

Figure S20 EDX analysis of **NiNPs/Me$_2$NHC@MXene** showing the presence of nickel. The presence of copper is from the grid used in HRTEM analysis.

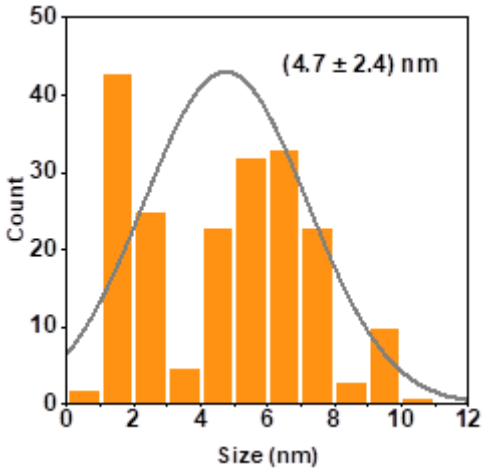

Figure S21 Size histogram of **NiNPs/Me$_2$NHC@MXene** (N = 100).

S10. Estimation of surface atoms in NiNPs/NHC@MXene nanoparticles

We estimate the number of surface Ni atoms considering a geometric approach based on the unit-cell Ni densities for NiO and β-$Ni(OH)_2$ of spherical nanoparticles composed of NiO:$Ni(OH)_2$ in a 70/30 ratio (obtained from XPS analysis). [4–6] The total Ni atoms in a particle of diameter *D* follow $N_{\mathrm{tot}} = (n\, V_{\mathrm{particle}}/ a^3)$, and the number of atoms in the outermost atomic layer is approximated as $N_{\mathrm{surf}} \approx \pi D^2/a^2$.

Table S2 Estimation of surface atoms

Data			
Parameter	Symbol	NiO	$Ni(OH)_2$
Lattice parameter (Å)	a	0.4176 nm	0.3126 nm
Crsytal system		cubic (rock salt)	hexagonal (brucite-type)
Ni atoms per unit cell	n	4	1
Unit cell volume (nm^3)	V_{cell}	0.0728	0.0392
Diameter of NiNPs from STEM	3.0 ± 0.8 nm		
Results			
Total Ni atoms	$N_{Ni,tot}$	570	
Surface Ni atoms	$N_{Ni,surf}$	212	
Dispersion factor	f	37%	

S11. Organic compound nomenclature

Table S3 Chemical structure and nomenclature used in this work.

Entry	Dehydrogenated		Hydrogenated	
1	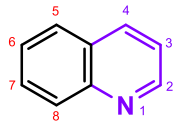	**1D**	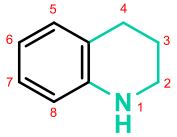	**1H**
2	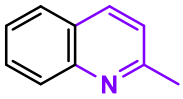	**2D**	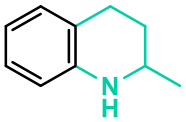	**2H**
3	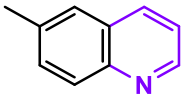	**3D**	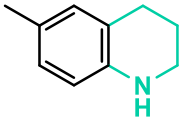	**3H**
4	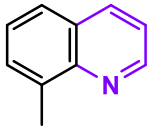	**4D**	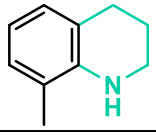	**4H**
5	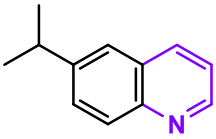	**5D**	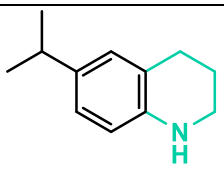	**5H**
6	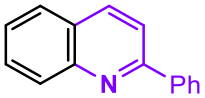	**6D**	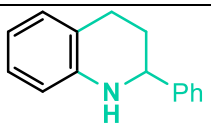	**6H**
7	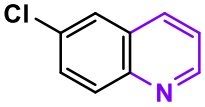	**7D**	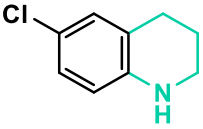	**7H**
8	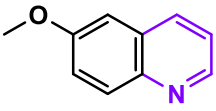	**8D**	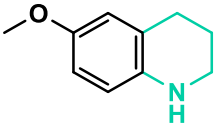	**8H**
9	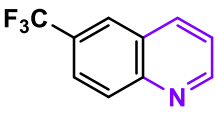	**9D**	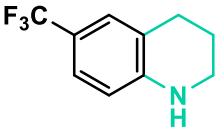	**9H**
10	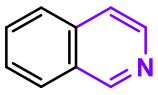	**10D**	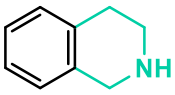	**10H**
11	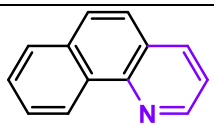	**11D**	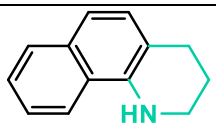	**11H**

S12. ^{1}H NMR spectra of crude reaction products

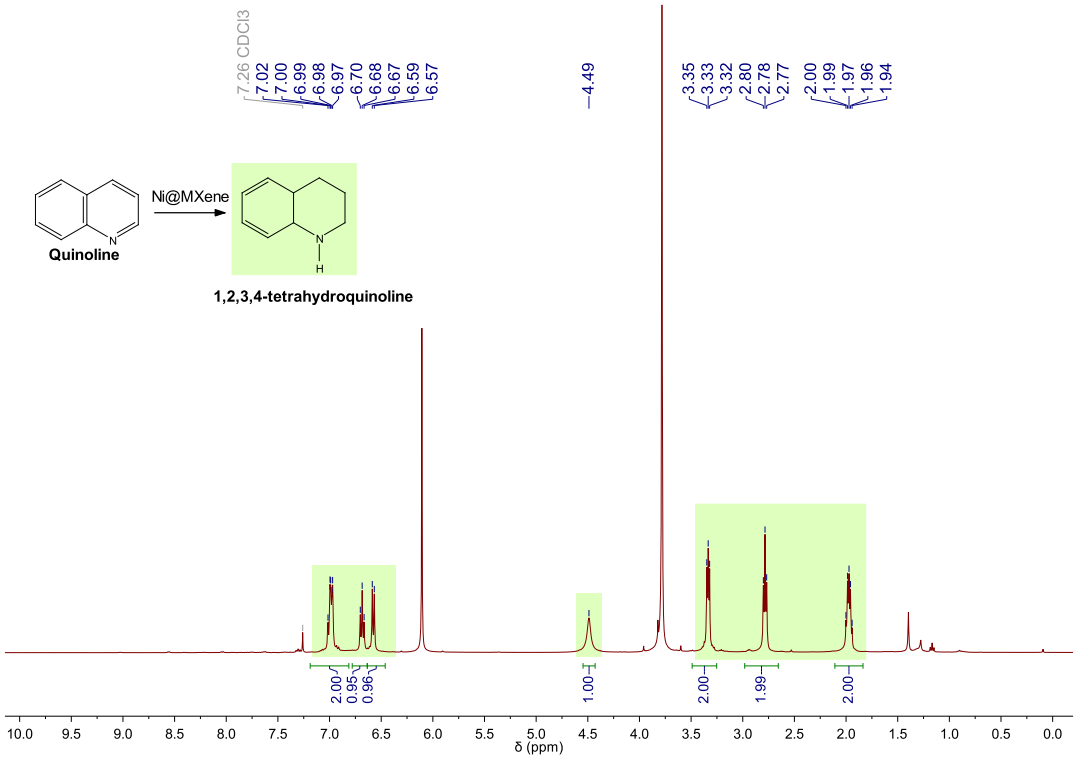

Figure S22 ^{1}H NMR spectrum of 1,2,3,4-tetrahydroquinoline (**1H**) in $CDCl_3$ in the presence of 1,3,5-trimethoxybenzene as an external standard (6.1 ppm and 3.75 ppm).

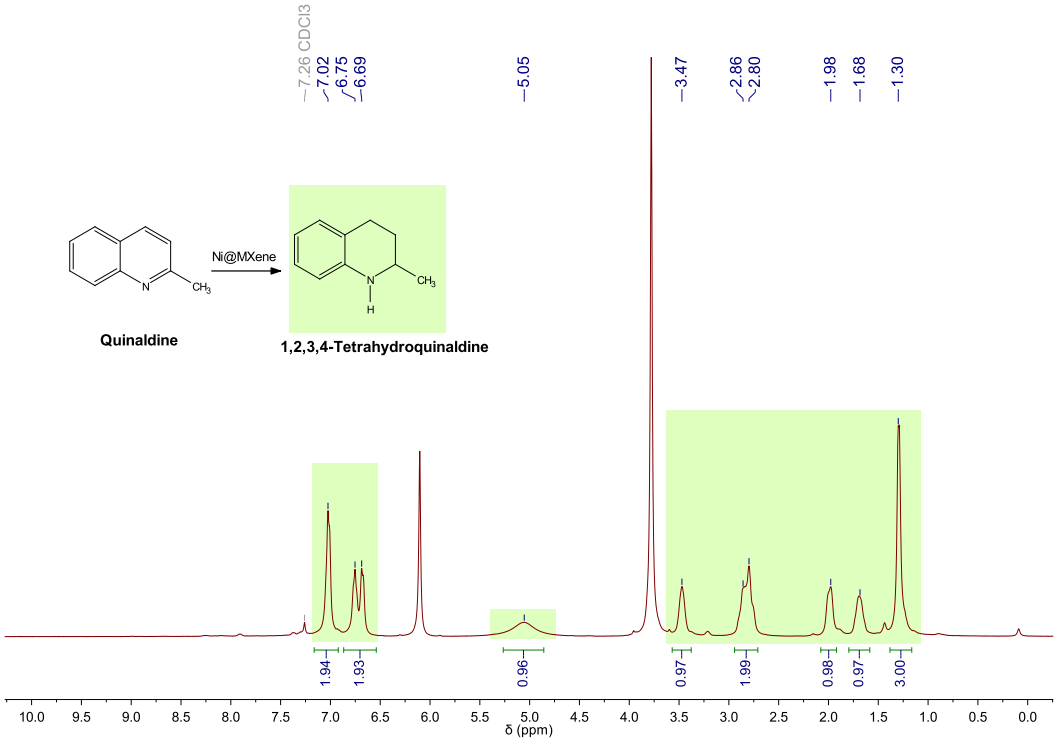

Figure S23 ^{1}H NMR spectrum of 1,2,3,4-tetrahydroquinaldine (**2H**) in $CDCl_3$ in the presence of 1,3,5-trimethoxybenzene as an external standard (6.1 ppm and 3.75 ppm).

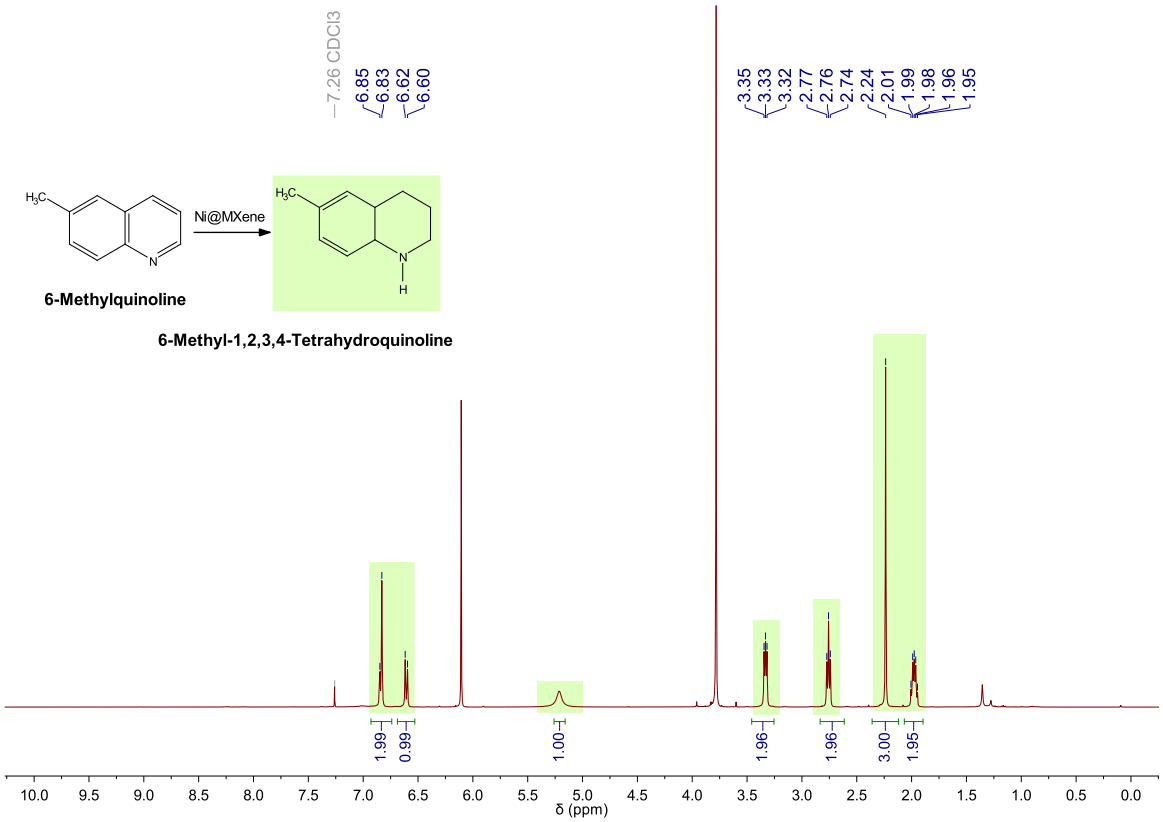

Figure S24 ^{1}H NMR spectrum of 6-methyl-1,2,3,4-tetrahydroquinoline (**3H**) in $CDCl_3$ in the presence of 1,3,5-trimethoxybenzene as an external standard (6.1 ppm and 3.75 ppm).

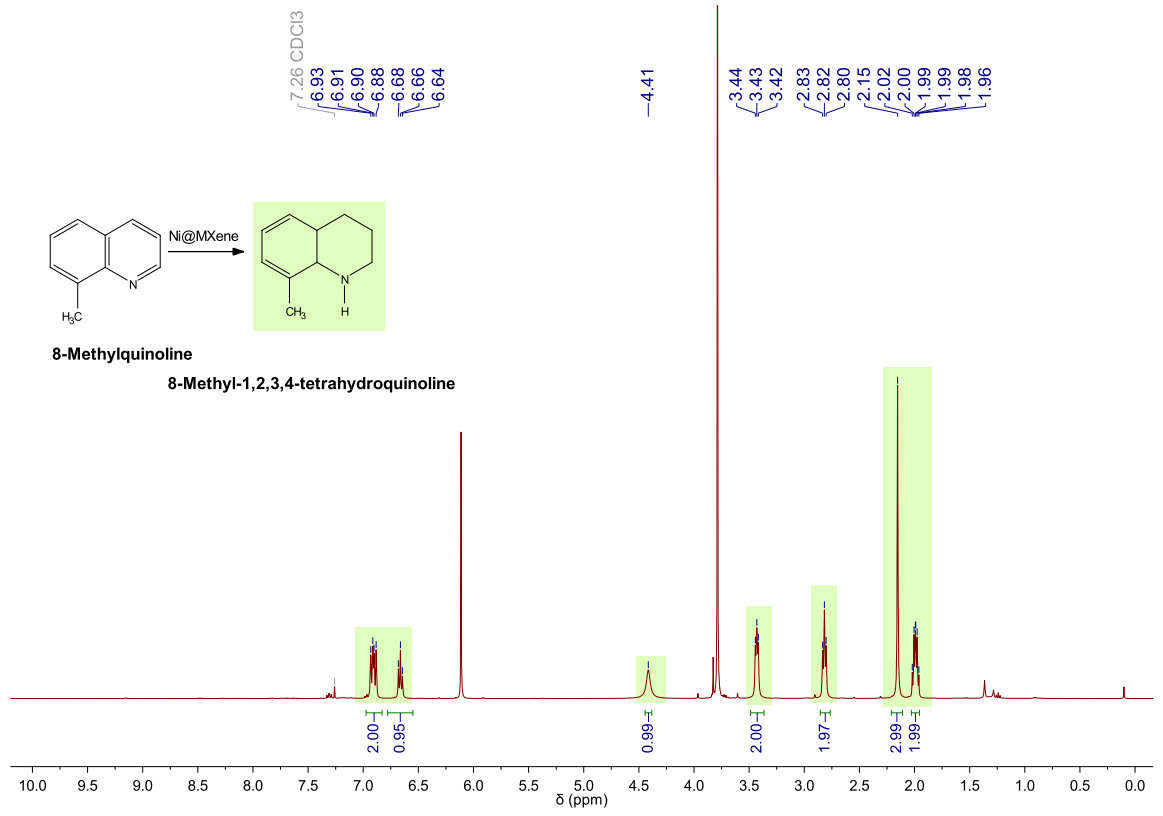

Figure S25 ^{1}H NMR spectrum of 8-methyl-1,2,3,4-tetrahydroisoquinoline (**4H**) in $CDCl_3$ in the presence of 1,3,5-trimethoxybenzene as an external standard (6.1 ppm and 3.75 ppm).

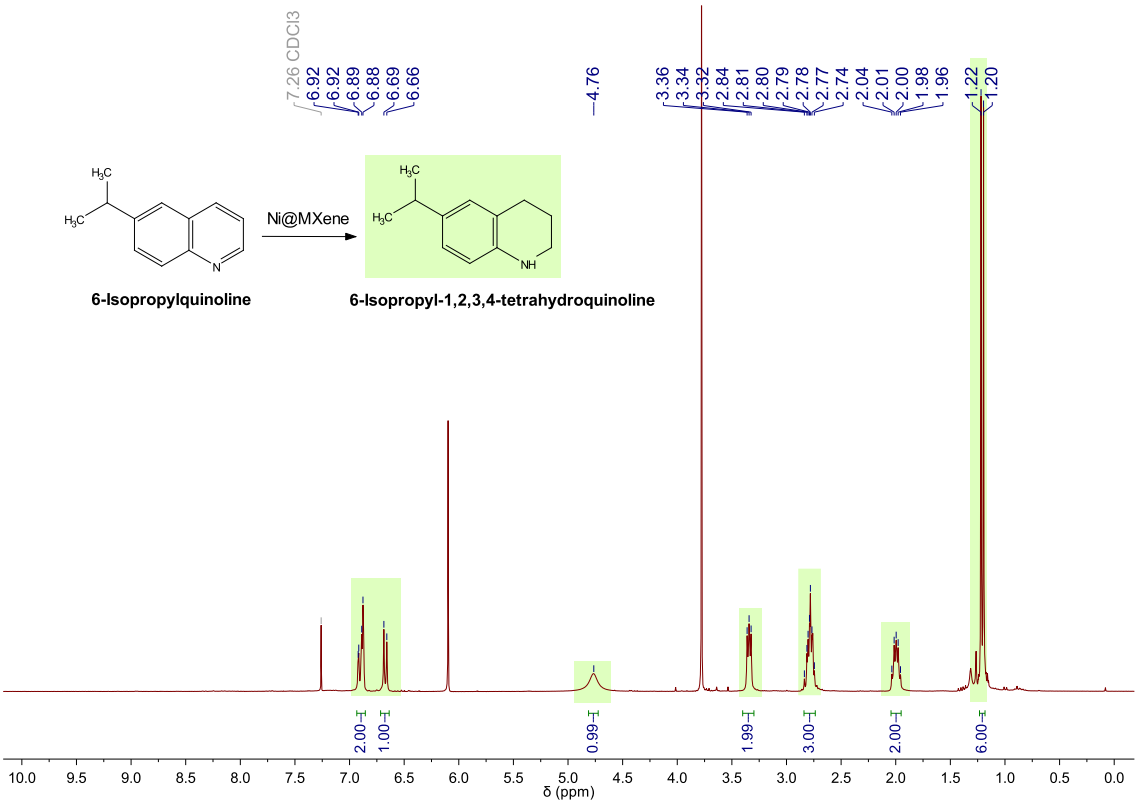

Figure S26 ^{1}H NMR spectrum of 6-isopropyl-1,2,3,4-tetrahydroquinoline (**5H**) in $CDCl_3$ in the presence of 1,3,5-trimethoxybenzene as an external standard (6.1 ppm and 3.75 ppm).

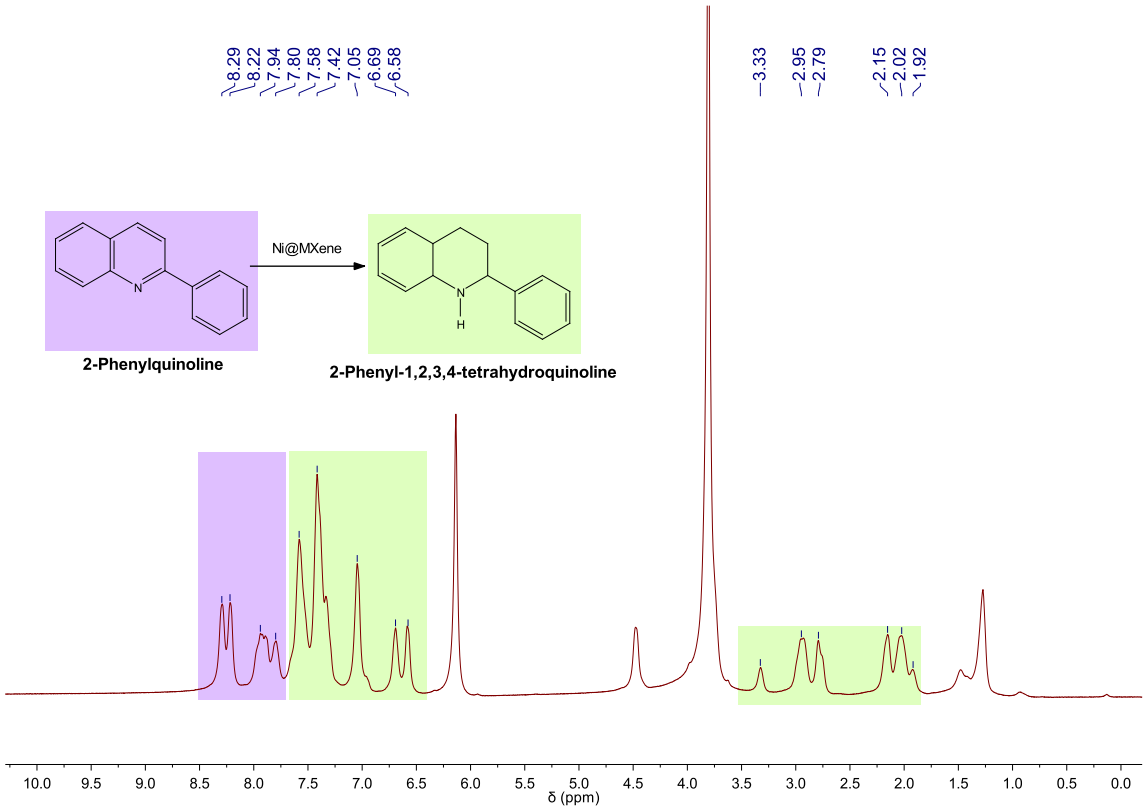

Figure S27 ^{1}H NMR spectrum of 2-phenylquinoline (**xi**) and 2-Phenyl-1,2,3,4-tetrahydroquinoline (**6H**) in $CDCl_3$ in the presence of 1,3,5-trimethoxybenzene as an external standard (6.1 ppm and 3.75 ppm).

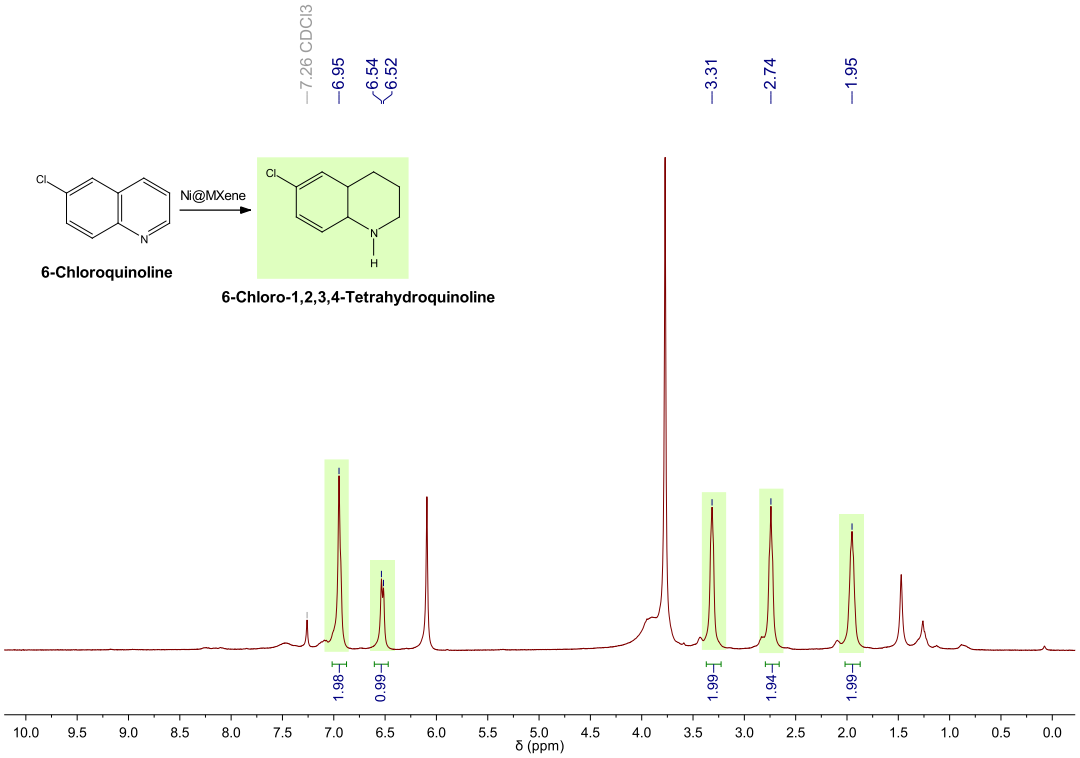

Figure S28 ^{1}H NMR spectrum of 6-chloro-1,2,3,4-tetrahydroquinoline (**7H**) in $CDCl_3$ in the presence of 1,3,5-trimethoxybenzene as an external standard (6.1 ppm and 3.75 ppm).

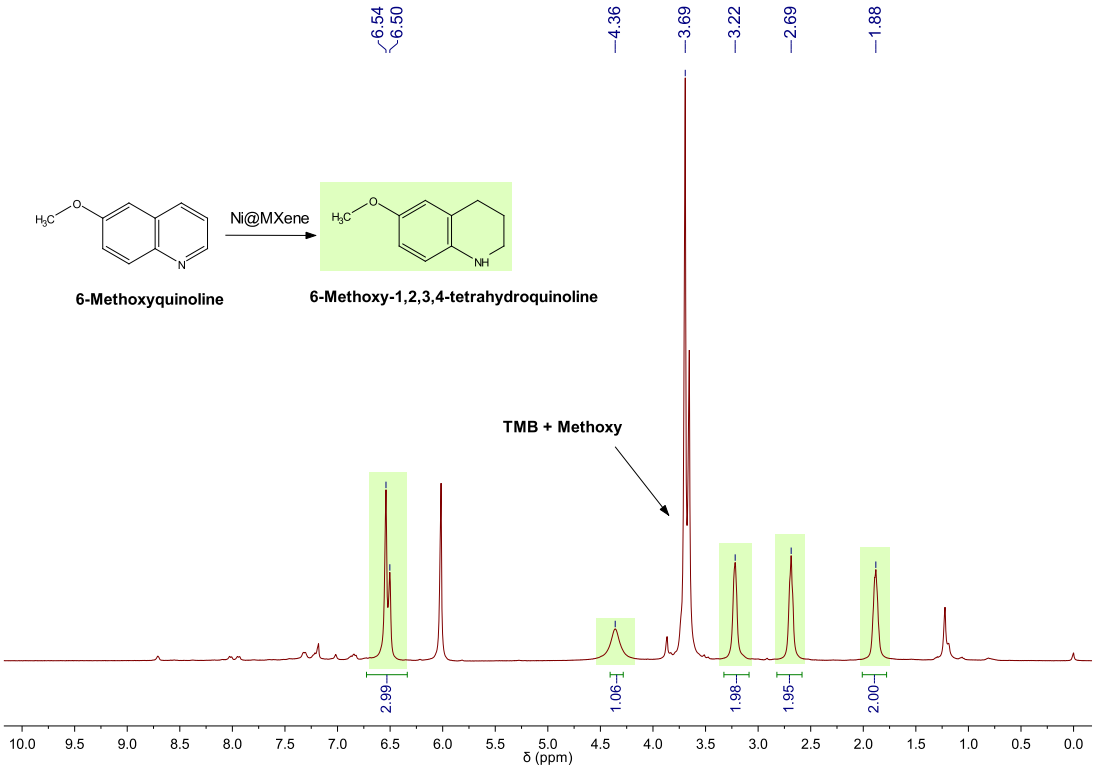

Figure S29 ^{1}H NMR spectrum of 6-Methoxy-1,2,3,4-tetrahydroquinoline (**8H**) in $CDCl_3$ in the presence of 1,3,5-trimethoxybenzene as an external standard (6.1 ppm and 3.75 ppm).

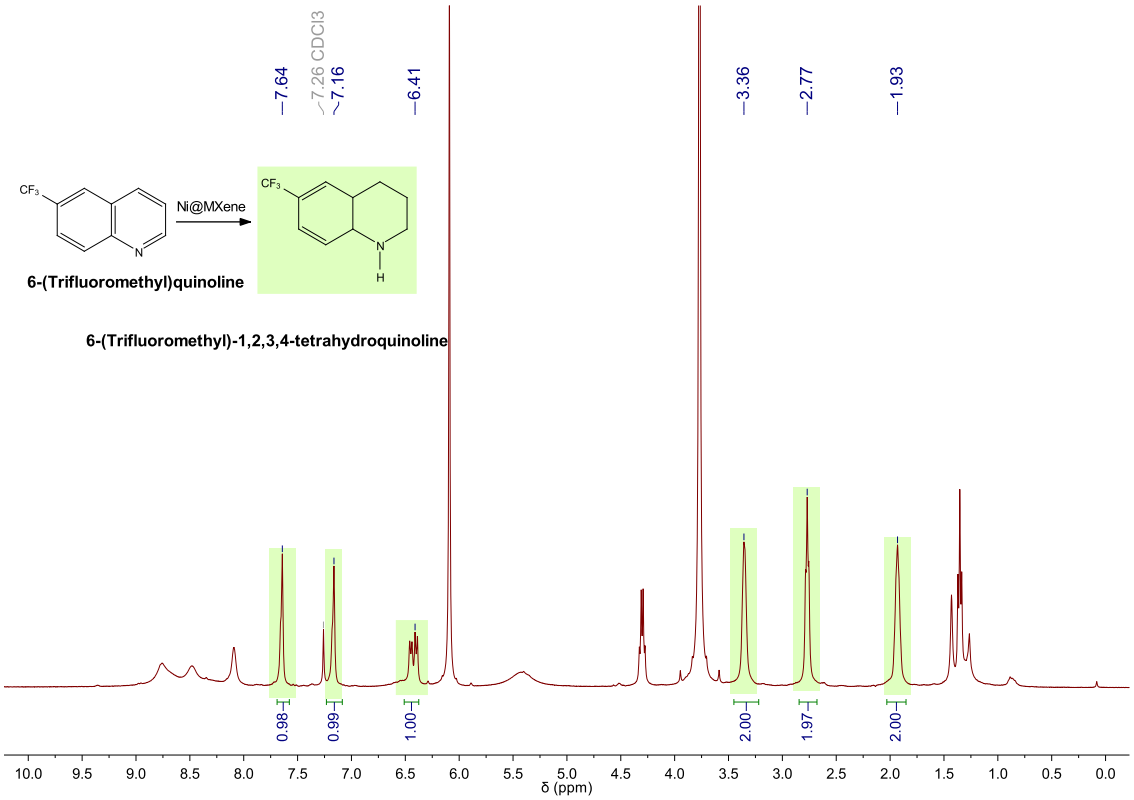

Figure S30 ^{1}H NMR spectrum of 6-(trifluoromethyl)-1,2,3,4-tetrahydroquinoline (**9H**) in $CDCl_3$ in the presence of 1,3,5-trimethoxybenzene as an external standard (6.1 ppm and 3.75 ppm).

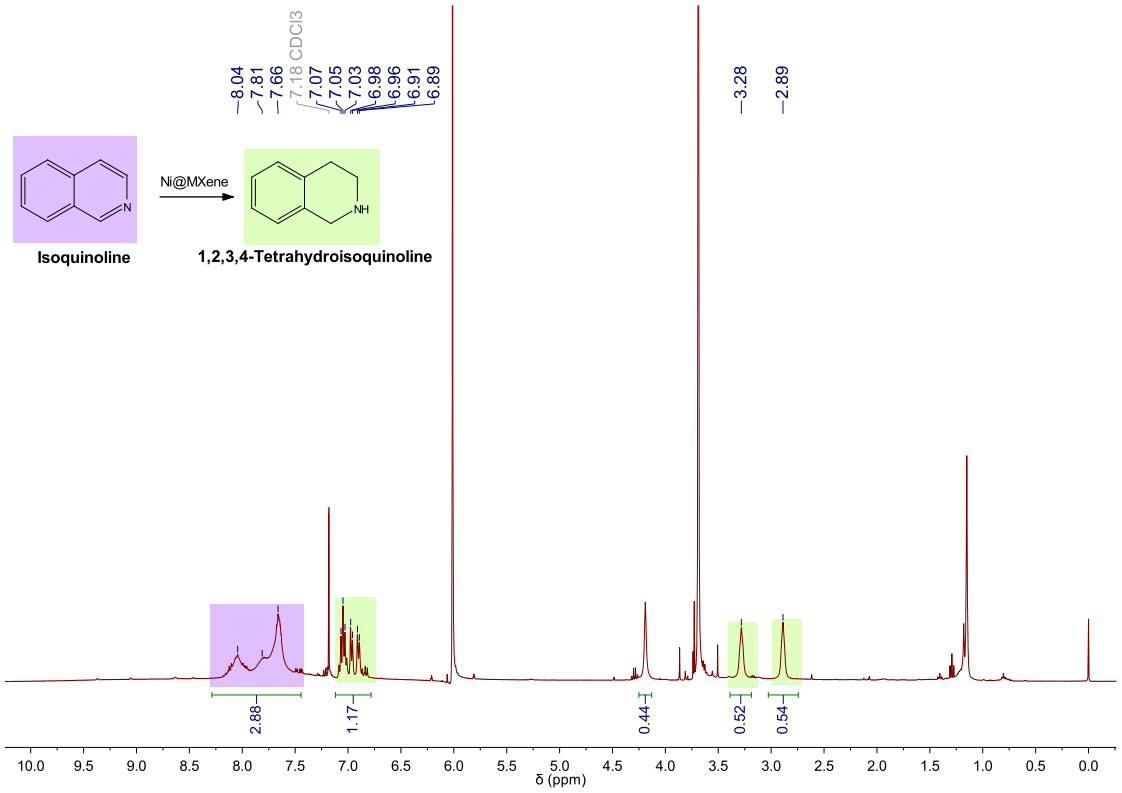

Figure S31 ^{1}H NMR spectrum of isoquinoline (**10D**) and 1,2,3,4-tetrahydroisoquinoline (**10H**) in $CDCl_3$ in the presence of 1,3,5-trimethoxybenzene as an external standard (6.1 ppm and 3.75 ppm).

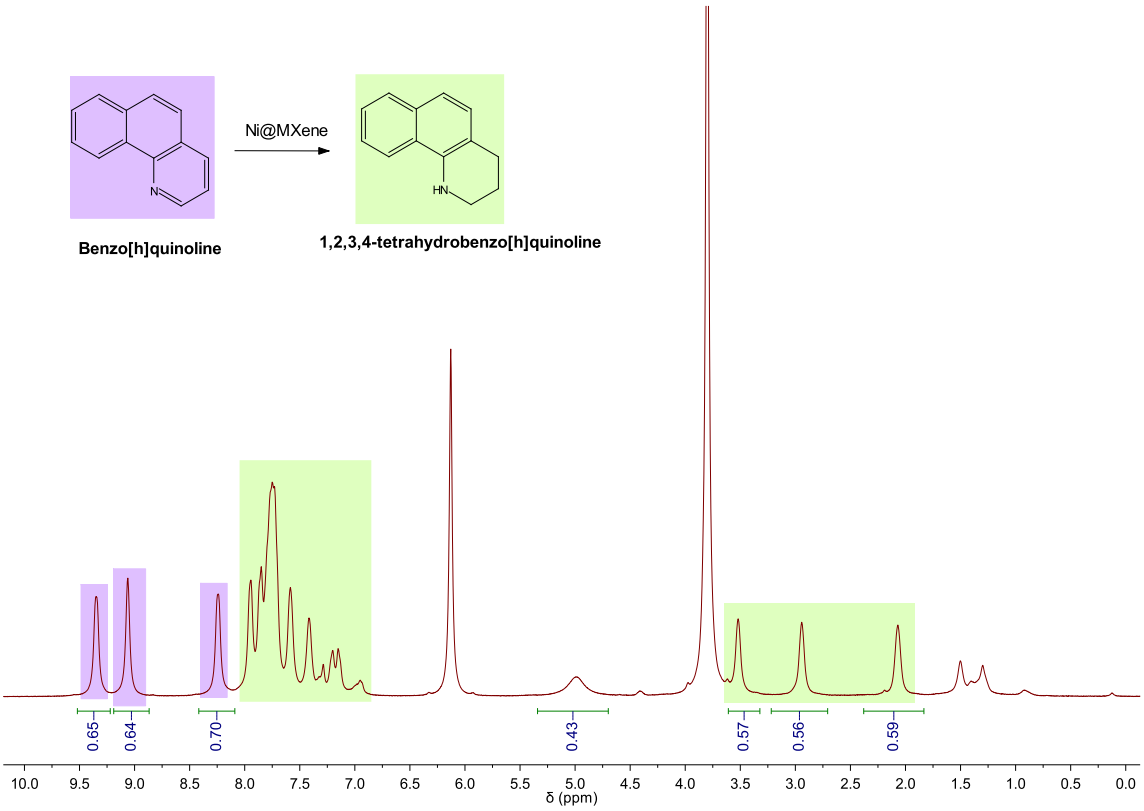

Figure S32 ^{1}H NMR spectrum of benzo[h]quinoline (**11D**) and 1,2,3,4-tetrahydrobenzo[h]quinoline (**11H**) in $CDCl_3$ in the presence of 1,3,5-trimethoxybenzene as an external standard (6.1 ppm and 3.75 ppm).

S13. X-ray photoelectron spectroscopy (XPS) of the spent catalytic material.

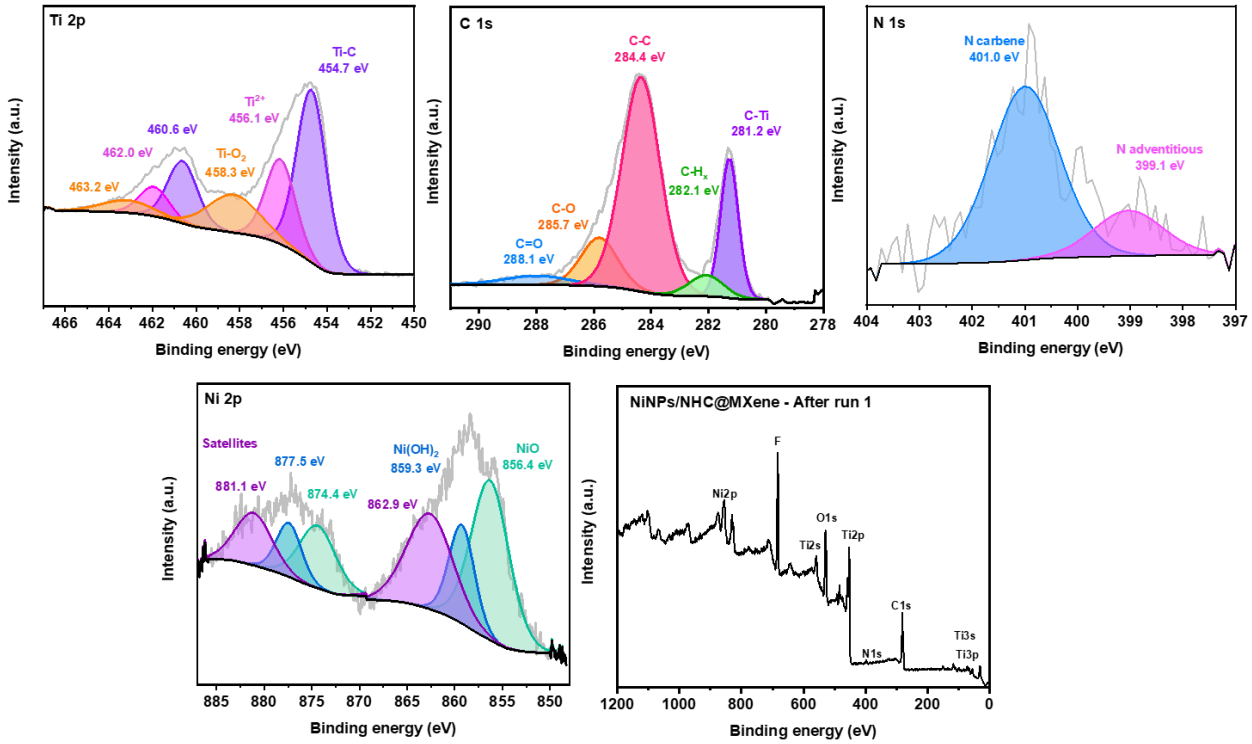

Figure S33 XPS analysis of the **NiNPs/NHC@MXene** after run 1.

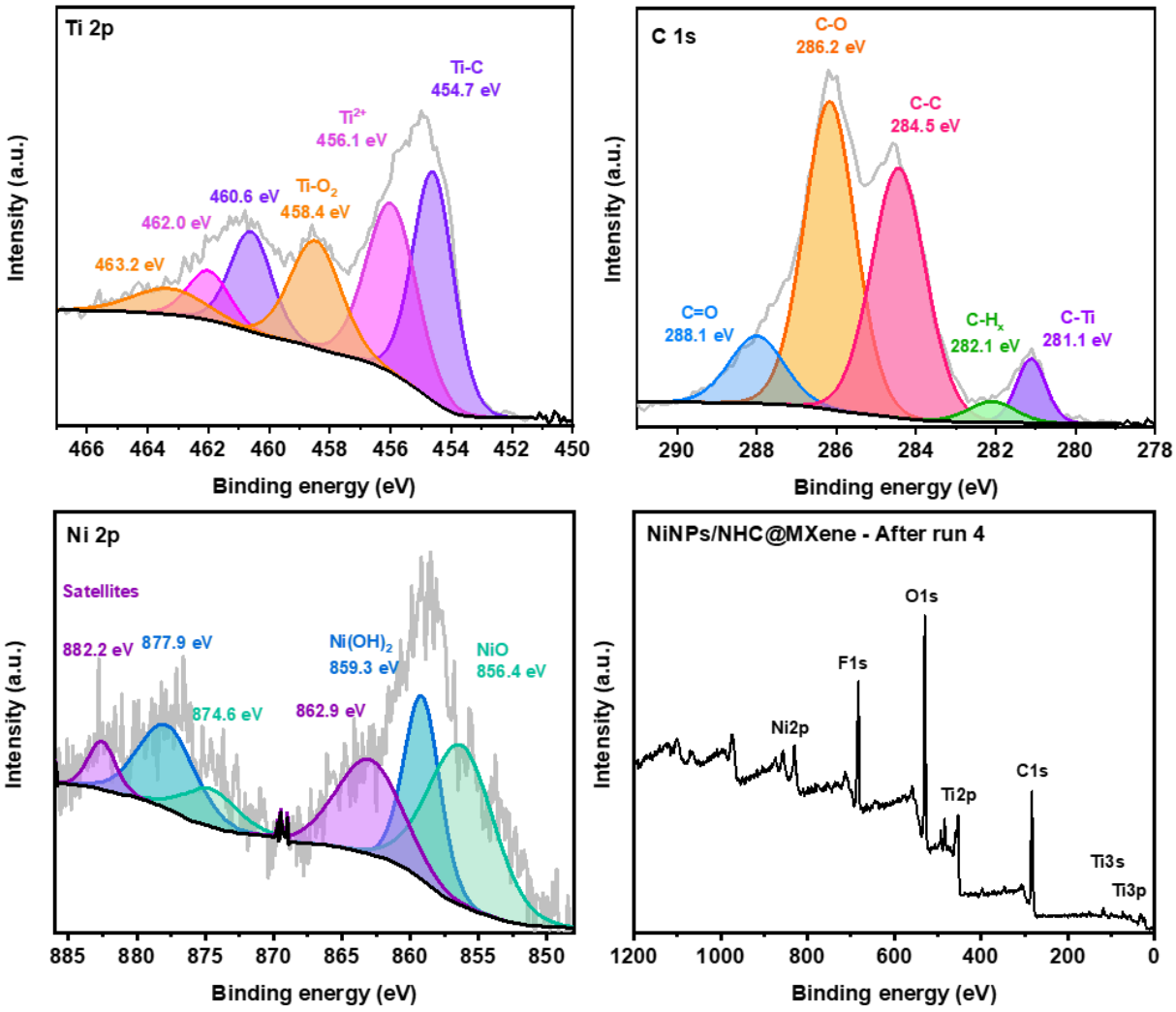

Figure S34 XPS analysis of the **NiNPs/NHC@MXene** after run 4.

S14. Summary of XPS assignments

Table S4 XPS peak assignments for the materials presented in this work.

Bonds		Binding energy (eV)				
		MAX Phase	**MXene**	**NiNPs/NHC@MXene**	**NiNPs/NHC@ MXene (after run 1)**	**NiNPs/NHC@ MXene (after run 2)**
Ti2p 3/2	Ti-C	454.0	455.2	454.5	454.7	454.7
	Ti-C-T_O		456.6			
	Ti-C-T_F		457.6			
	Ti^{2+}	455.6		456.0	456.1	456.1
	Ti=O	458.3		457.6	458.3	458.4
Ti2p 1/2	Ti-C	460.0	460.8	460.1	460.6	460.6
	Ti-C-T_O		462.1			
	Ti-C-T_F		463.2			
	Ti^{2+}	462.7		461.3	462.0	462.0
	Ti=O	464.2		462.3	463.3	463.2
C1s	C-Ti	281.0	281.9	281.1	281.2	281.1
	C-H_x	282.2		282.1	282.1	282.1
	C-C	284.5	284.6	284.5	284.4	284.5
	C-O	286.1	286.1	285.7	285.7	284.2
	O-C=O	288.6		288.5	288.1	288.1
Al 2s	Al^0	116.5				
	Al_2O_3	118.9				
Ni2p 3/2	NiO			856.4	856.4	856.4
	$Ni(OH)_2$			859.3	859.3	859.3
	Satellites			862.9	862.9	862.9
Ni2p 1/2	NiO			874.3	874.4	874.6
	$Ni(OH)_2$			877.5	877.5	877.9
	Satellites			881.1	881.1	882.2
O1s	TiO_2	530.0	530.0			
	C=O	531.0				
	C-O	531.9				
	Al_2O_3	533.0				
	O_{fcc}		532.0			
	C-OH		533.0			
	H_2O		534.4			
F1s	F^-		683.4			
	Ti-F		685.1			
	O-Ti-F		686.9			
	C-F		688.5			
Br				182.0		
				188.6		
N	N adv			399.4	399.1	
	N carbene			401.2	401.0	

S15. References

1 J. Medina-Vargas, A. Mollar-Cuni, S. Martín, I. Sorribes and J. A. Mata, Graphene as a Suitable Support for Nickel Nanoparticles Functionalized with NHC Ligands in Dehydrogenation of Alcohols, *ChemCatChem*, 2025, 17, e202500490.

2 S. Sabater, J. A. Mata and E. Peris, Catalyst enhancement and recyclability by immobilization of metal complexes onto graphene surface by noncovalent interactions, *ACS Catal*, 2014, 4, 2038–2047.

3 V. Ritleng, C. Barth, E. Brenner, S. Milosevic and M. J. Chetcuti, Synthesis, Structure, and Solution Dynamics of Pentamethylcyclopentadienyl Nickel Complexes Bearing N-Heterocyclic Carbene Ligands, *Organometallics*, 2008, 27, 4223–4228.

4 Y. D. Gamburg, Fraction of Surface Atoms in the Nanoparticles and Critical Nuclei of a New Phase, *Russian Journal of Physical Chemistry A*, 2022, 96, 135–138.

5 C. N. R. Rao, G. U. Kulkarni, P. J. Thomas and P. P. Edwards, in *Trends in Chemistry of Materials*, Co-Published with Indian Institute of Science (IISc), Bangalore, India, 2008, pp. 435–441.

6 F. Baletto and R. Ferrando, Structural properties of nanoclusters: Energetic, thermodynamic, and kinetic effects, *Rev Mod Phys*, 2005, 77, 371–423.

7 V. Vermaak, H. C. M. Vosloo and A. J. Swarts, Fast and Efficient Nickel(II)-catalysed Transfer Hydrogenation of Quinolines with Ammonia Borane, *Adv Synth Catal*, 2020, 362, 5788–5793.

8 L. Niu, Y. An, X. Yang, G. Bian, Q. Wu, Z. Xia and G. Bai, Highly dispersed Ni nanoparticles encapsulated in hollow mesoporous silica spheres as an efficient catalyst for quinoline hydrogenation, *Molecular Catalysis*, 2021, 514, 111855.

9 V. Goyal, T. Bhatt, A. Kuttasseri, A. Mahata, R. Zbořil, K. Natte and R. V. Jagadeesh, A biomass-derived nickel-based nanomaterial as a sustainable and reusable catalyst for hydrogenation of arenes and heteroarenes, *RSC Sustainability*, 2025, 3, 2235–2245.

10 Z. Yuan, X. Li, G. Wang, Z. Zhu, Y. Liao, Z. Zhang and B. Liu, Efficient hydrogenation of N-heteroarenes into N-heterocycles over MOF-derived CeO2 supported nickel nanoparticles, *Molecular Catalysis*, 2023, 540, 113052.

11 P. Ryabchuk, G. Agostini, M.-M. Pohl, H. Lund, A. Agapova, H. Junge, K. Junge and M. Beller, Intermetallic nickel silicide nanocatalyst—A non-noble metal–based general hydrogenation catalyst, *Sci Adv*, 2018, 4, eaat0761.

12 S. Mao, P. Ryabchuk, S. Dastgir, M. Anwar, K. Junge and M. Beller, Silicon-Enriched Nickel Nanoparticles for Hydrogenation of N-Heterocycles in Aqueous Media, *ACS Appl Nano Mater*, 2022, 5, 5625–5630.

13 Y. Hu, M. Liu, S. Bartling, H. Lund, H. Atia, P. J. Dyson, M. Beller and R. V. Jagadeesh, A general and robust Ni-based nanocatalyst for selective hydrogenation reactions at low temperature and pressure, *Sci Adv*, DOI:10.1126/sciadv.adj8225.

14 R. Yun, W. Ma, L. Hong, Y. Hu, F. Zhan, S. Liu and B. Zheng, Ni@PC as a stabilized catalyst toward the efficient hydrogenation of quinoline at ambient temperature, *Catal Sci Technol*, 2019, 9, 6669–6672.